Distribution System Operation Amidst Wildfire-Prone Climate Conditions Under Decision-Dependent Line Availability Uncertainty

Alexandre Moreira, *Member, IEEE,* Felipe Piancó, *Student Member, IEEE,* Bruno Fanzeres, *Member, IEEE,* Alexandre Street, *Senior Member, IEEE,* Ruiwei Jiang, Chaoyue Zhao, and Miguel Heleno, *Senior Member, IEEE*

***Abstract*—Wildfires can severely damage electricity grids leading to long periods of power interruption. Climate change will exacerbate this threat by increasing the frequency of dry weather conditions. Under these climate conditions, human-related actions that initiate wildfires should be avoided, including those induced by power systems operation. In this paper, we propose a novel optimization model that is capable of determining appropriate network topology changes (via switching actions) to alleviate the levels of power flows through vulnerable parts of the grid so as to decrease the probability of wildfire ignition. Within this framework, the proposed model captures the relationship between failure probabilities and line-flow decisions by explicitly considering the former as a function of the latter. The resulting formulation is a two-stage model with endogenous decision-dependent probabilities, where the first stage determines the optimal switching actions and the second stage evaluates the worst-case expected operation cost. We propose an exact iterative method to deal with this intricate problem and the methodology is illustrated with a 54-bus and a 138-bus distribution system.**

***Index Terms*—Decision-dependent uncertainty, wildfire in distribution systems, distribution system operation, ambiguity aversion, line switching.**

NOMENCLATURE

Sets

$\mathcal{L}$	Set of indexes of line segments.
$\mathcal{L}^{sw}$	Set of indexes of switchable line segments.
$\mathcal{K}^{forbid}$	Set of indexes of forbidden switching patterns.
$\mathcal{N}$	Set of indexes of buses.
$\mathcal{N}^{subs}$	Set of indexes of buses with substation.

Parameters

β_l	Sensitivity of failure probability to the scheduled active power flow of line $l \in \mathcal{L}$.
γ_l	Estimated upper bound for the nominal probability of failure associated with line $l \in \mathcal{L}$.
$C^{ll,p+}$	Cost of active power surplus.
$C^{ll,p-}$	Cost of active power loss.
$C^{ll,q+}$	Cost of reactive power surplus.
$C^{ll,q-}$	Cost of reactive power loss.
C_l^{sw}	Cost of switching line $l \in \mathcal{L}^{sw}$.
C_b^{tr}	Cost of active power from main transmission grid for bus $b \in \mathcal{N}^{subs}$.
D_b^p	Active power demand at bus $b \in \mathcal{N}$.
E_l	Number of digits for binary expansion used in Master problem linearization for line $l \in \mathcal{L}$.
$\overline{F}_l$	Maximum power flow at line $l \in \mathcal{L}$.
$\overline{P}_b^{tr}$	Maximum active power injection at bus $b \in \mathcal{N}^{subs}$.
PF_b	Power factor at bus $b \in \mathcal{N}$.
$\overline{Q}_b^{tr}$	Maximum reactive power at bus $b \in \mathcal{N}^{subs}$.
$\underline{Q}_b^{tr}$	Minimum reactive power at bus $b \in \mathcal{N}^{subs}$.
R_l	Resistance of line $l \in \mathcal{L}$.
s	Step for binary expansion used in Master problem linearization.
$\underline{V}_b$	Voltage lower bound at bus $b \in \mathcal{N}$.
$\overline{V}_b$	Voltage upper bound at bus $b \in \mathcal{N}$.
V^{ref}	Voltage reference.
X_l	Reactance of line $l \in \mathcal{L}$.
$z_l^{sw,0}$	Initial switching status of line $l \in \mathcal{L}^{sw}$.

Decision Variables

α	Worst-case expected value of the lower-level problem.
ΔD_b^{p-}	Amount of active power loss at bus $b \in \mathcal{N}$.
ΔD_b^{p+}	Amount of active power surplus at bus $b \in \mathcal{N}$.
ΔD_b^{q-}	Amount of reactive power loss at bus $b \in \mathcal{N}$.
ΔD_b^{q+}	Amount of reactive power surplus at bus $b \in \mathcal{N}$.
f_l^p	Active power flow at line $l \in \mathcal{L}$.
f_l^q	Reactive power flow at line $l \in \mathcal{L}$.
p_b^{tr}	Amount of active power injected at bus $b \in \mathcal{N}^{subs}$.
q_b^{tr}	Amount of reactive power at bus $b \in \mathcal{N}^{subs}$.
$v_b^\dagger$	Squared voltage at bus $b \in \mathcal{N}$.
y_l^{sw}	Binary decision variable indicating a switching action of line $l \in \mathcal{L}^{sw}$ (1 if switched, 0 otherwise).
z_l^{sw}	Binary decision variable of switching status of line $l \in \mathcal{L}^{sw}$ (1 if switched on, 0 otherwise).

I. INTRODUCTION

WILDFIRE events are a real threat to power systems operations at both transmission and distribution levels. The damage caused by these events might cost a significantly large amount of irrecoverable capital to society (e.g., the estimate of more than $700 million in damage to transmission and distribution systems over 2000-2016 [1]) and be irreparable in cases when human lives are involved. Over the past two decades, California, for instance, has experienced a large raise in the frequency of small wildfires, while the total burned area from large ones has also substantially increased [2]. In this context, human-induced activities have been placed at a top rank among the main roots of wildfire ignition, with power system operations responsible for some of them, as, for instance, when eventual sparks due to power flow through overhead lines aligned with dry weather conditions and strong wind speed levels cause this natural disaster [3]. In extreme cases, this has been addressed by the electric sector with public safety power shut-offs (PSPS), which results in significant load sheddings and economic impacts [4]. As a consequence, novel operative policies are of significant importance in order to establish efficient power system operations amidst wildfire-prone climate conditions, assuring thus high levels of sustainability and system resilience [5], [6].

Due to this critical prospect, various research efforts have been dedicated to addressing resilience in power systems under potential natural disasters and human-made attacks. At the transmission level, for example, the work developed in [7] proposes a two-stage stochastic Mixed-Integer Nonlinear Programming (MINLP) model to define investment strategies to improve resilience, considering a range of earthquake events. The methodology developed by [8] combines optimization and simulation techniques to determine a portfolio of investments to improve grid resilience while also considering the potential occurrence of earthquakes. At the distribution level, on the other hand, the work reported in [9] presents a storage sitting and sizing model to increase resilience while facing seismic hazards. In [10], the authors design a three-level system of optimization models to identify line hardening solutions to protect the distribution grid against intentional or unintentional attacks. Particularly regarding wildfires, an increasing deal of attention has been emerging in technical literature. Notably, in [11], the authors propose a methodology to alleviate wildfire risks by optimizing the selection of components in the grid to be de-energized in a power shut-off scheme. In [12], a stochastic programming model that aims at increasing the resiliency of a distribution system exposed to an approaching wildfire is devised under exogenous uncertainties such as solar radiation, wind speed, and wind direction. In [13], the authors claim that, during wildfires, the behavior of energy consumers can change, and this change will be exacerbated as the adoption of electric vehicles (EV) grows. So, the work developed in [13] aims to quantify the resilience of power grids under the presence of EVs given the available generation. In [14], microgrids and distributed energy resources (DERs) are referred to as potential alternatives to alleviate the impact of wildfires and real cases are used as examples to support this point of view. In [15], a Markov decision-process-based approach is proposed to determine optimal generation decisions during wildfire progression. In [16], the authors define 3 lines of defense for wildfire risk management and provide a literature review for each of these lines. The first line is associated with wildfire prevention and includes wildfire detection and vegetation management. The second line is related to wildfire risk mitigation and comprises actions such as preemptive de-energization and grid operations management. The third line involves recovery preparedness and, within this context, recovery logistics, energy contingency plans, disaster risk financing and community engagement are mentioned. Notwithstanding the relevance of recent technical literature, none of them takes into account the direct impact of the power flow dispatch on the likelihood of line failures in a decision-dependent uncertainty (DDU) framework.

In this work, we propose a methodology that contributes to the second line of defense mentioned in [16]. Despite the relevant contributions of the aforementioned papers, none of them explicitly considers the impact of power flow levels on the failure probabilities of line segments due to a potential ignition of a wildfire. To the best of our knowledge, this DDU relationship in the context of wildfires is captured for the first time within an optimal power flow operational model by our proposed methodology in this paper. Although more actions, such as vegetation management, could be considered to decrease the risk of wildfires, for simplicity purposes and to keep the contribution of the paper focused on the DDU representation of the interaction between power flows and wildfires, we only consider operational topology changes as potential measures to alleviate the risk of igniting a wildfire.

Line switching and reconfiguration are frequently considered as measures to deal with events that challenge the resilience of power systems. For the transmission level, [17] proposes an investment planning methodology that includes switches as candidate options to increase resilience. For the distribution level, switches are also considered as candidate investment options to deal with disaster scenarios in [18]. Furthermore, in the context of wildfires, the work developed in [19] indicates that lower overall investment costs are needed to make the system more resilient if new lines are included and switching is allowed. In addition, according to [20], the Californian utility San Diego Gas & Electric decided to install switching devices in an effort to better deal with wildfire events. Moreover, from the operational perspective, [21]–[26] mention switching as a relevant maneuver to improve resilience and alleviate the impacts of extreme events.

From a modeling perspective, it is important to emphasize that uncertainties in power system operations are typically exogenously induced into the decision-making process. In this framework, uncertainty sources are solely associated with external factors and are not endogenously affected by operational actions. However, in many realistic cases, such as under wildfire-prone climate conditions, the operation of electric grids is also associated with the origin of fire ignitions, which significantly increase line failure probabilities. Due to this double role of power grids, the nature of the uncertainty is thus more complex to characterize (dependent not only on meteorological conditions – exogenous factors, but also on the grid operation decisions – endogenous factors), challenging the standard exogenously-induced approach. Therefore, in order to design resilience-oriented operational strategies in high fire-threat areas, utility operators must be aware of the impact of their operational decisions on the likelihood of wildfire initiation and reduction in reliability levels[1], i.e., the endogenous nature of the uncertainty.

There are two major categories of frameworks to model decision-dependent uncertainty. In the first one, there are different subsets of uncertainty realizations and, depending on the action(s) of the decision-maker, uncertainty realizations within a particular subset will be allowed to materialize while others that do not belong to this subset will be discarded. In the classic example of gas field developments [28], the size (amount of gas that can be produced) of a particular field can be uncertain before an attempt of production starts. In this case, the two main outcomes for a decision-maker are (i) being able to profit from the field or (ii) not being able to profit. While the second outcome is the only one possible if the decision-maker does not start to exploit the field, the first outcome may be observed only if the decision is to exploit the field. In this case, the actions of the decision-maker clearly impact the resolution of uncertainty. In the second category of decision-dependent uncertainty framework, there is only one set of potential uncertainty realizations and, in this

[1]We refer to [27] and the references therein for a wider discussion on the impact of distribution system operations in the probabilistic characterization of wildfire ignition.

case, the action(s) of the decision-maker may render particular uncertainty realizations more or less likely to materialize by modifying their probabilities of occurrence. In [29], for example, the authors model generation expansion while considering that investments in wind generation capacity can affect the probabilities of electricity prices whose sample space is fixed and known. Our proposed methodology in this paper also assumes a fixed and known sample space and considers that decision variables associated with power flows can influence the probabilities of line failures. Therefore, our methodology falls into the second aforementioned category of decision-dependent uncertainty framework. This modeling choice is motivated by the occurrence of wildfires started by power lines in different parts of the world which resulted in serious consequences including the disruption of power distribution systems [30].

In this paper, we leverage the second modeling type to propose a new methodology for distribution system operations capable of endogenously taking into account the impact of power flows on failure probabilities in the context of a potential wildfire event. We design a decision-dependent uncertainty framework where the line failure probabilities are a function (dependent) of the power flow levels. In this framework, we consider that during adverse climate conditions (dry weather and reasonably strong wind), switching actions can be made to reduce power flows in vulnerable areas of the grid, therefore decreasing the probability of wildfire ignition and consequent line failures, while seeking to maintain load supply. Thus, the proposed methodology allows distribution system operators to perform efficient switching actions to improve the system reliability accounting for decision-dependent line availability uncertainty. Structurally, the proposed methodology falls into the class of a two-stage, distributionally robust optimization problem with decision-dependent uncertainty [31]. In the first stage, our model decides the network topology (switching lines) and power imports from the main grid with main goal of minimizing the operational cost in the pre-contingency state plus the worst-case expected cost of operating the system under post-contingency states considering probabilities adjusted according to the pre-contingency network topology and line power flows. Then, in the second stage, the power flow and energy not served are evaluated for each post-contingency state.

Although the focus in the paper is on the endogenous impact of power flows on line failure probabilities, our methodology is general enough to accommodate exogenous factors that also affect these probabilities. For instance, wind speeds higher than 20 m/s can impact the probability of failure of class 5 southern pine poles (popular in the US) depending on age and leaning angle [32]. Also, drought, under low or high winds, can enable circumstances for the occurrence of a wildfire [33]. In our proposed methodology, line failure probabilities are bounded by affine functions of the power flows through the lines. In this case, the user has the flexibility to set the intercept of these affine functions according to the corresponding wind fragility curves [32] and/or any other aspect that might influence line failure probabilities regardless of the power flows. Moreover, adverse climate conditions including drought as well as proximity and condition of vegetation can be incorporated into the model via the slope of the affine function associated with line failure probabilities. It is worth mentioning that we consider that failure probabilities can vary up to the upper bounds defined by the aforementioned affine functions as it is, in general, nontrivial to estimate failure probabilities of line segments in distribution networks [34] and, therefore, we resort to the framework of distributionally robust optimization to appropriately characterize this probability-ambiguous context.

To summarize, the contributions of this paper are twofold:

1) To formulate the distribution grid operation under adverse climate conditions as a two-stage distributionally robust optimization problem where the probabilities of line failure are co-dependent on the weather conditions (exogenous) and system power flows (endogenous). In the first stage, the system operator decides switching actions (therefore determining grid topology) and power imports from the main grid aiming at co-optimizing the pre-contingency and the worst-case expected post-contingency operations, formulated as the second stage.
2) To devise an effective decomposition-based solution methodology capable of solving the proposed optimization problem. The approach is able to circumvent the computational difficulties posed by the multi-level (non-convex) structure intrinsic to the decision-dependent uncertainty modeling frameworks.

II. Optimal Distribution System Operation with Decision-Dependent Uncertainty

The main objective of this work is to propose a methodology to determine the least-cost operation of a distribution system taking into account the impact of operative decisions in the probabilistic characterization of the line availability. We assume that the operator can perform switching actions in a set of line segments in the distribution system with the objective of minimizing the worst-case expected operation cost considering a decision-dependent uncertainty in line availability. Although we recognize that there exist distribution systems operated as meshed networks (most in densely urban areas), we follow current practices in both technical literature and actual distribution system operation, and impose system radiality constraints when prescribing the system reconfiguration (i.e., line switching decision) [35]. Technically, such topological operating characteristics stem from a variety of reasons, such as the ease in coordination, protection, and system reconfiguration (e.g., line switching), as well as the potential reduction in short-circuit current [36]. Structurally, the proposed methodology falls into the class of a two-stage distributionally robust optimization problem with decision-dependent uncertainty [31]. In the first stage, our model decides the network topology (switching lines) that maintains the system radiality condition and power imports from the main grid. The primary goal is to minimize the operational cost in the pre-contingency state plus the worst-case expected cost of operating the system under post-contingency states considering probabilities adjusted according to the pre-contingency network topology and line power flows. Then, in the second stage, the power flow and energy not served are evaluated for each post-contingency state. Fig. 1 depicts an illustrative outlook of the proposed distribution system operation methodology as a two-stage decision-making process and its mathematical characterization as a three-level system of nested optimization problems.

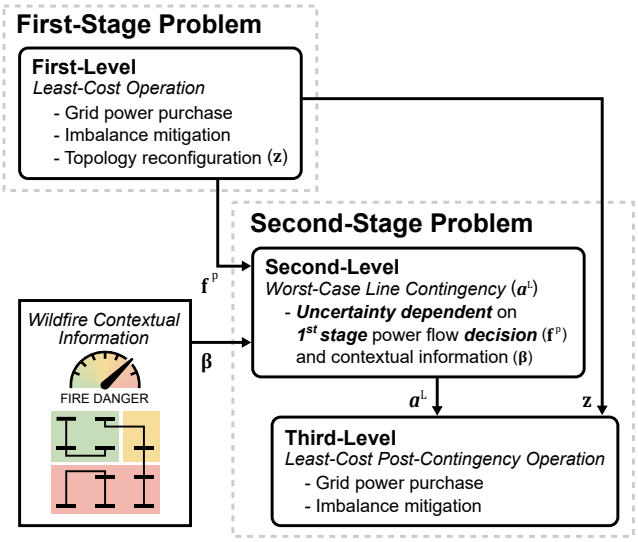

Fig. 1. Outlook of the proposed distribution system operation methodology as a two-stage decision-making process with mathematical characterization as a three-level system of nested optimization problems.

In (1)–(25), the proposed distribution system operation model is formulated:

$$\underset{\substack{\Delta D_b^{p+},\Delta D_b^{p-},\Delta D_b^{q+},\Delta D_b^{q-},\\ f_l^p,f_l^q,p_b^{tr},q_b^{tr},v_b^{\dagger},y_l^{sw},z_l^{sw}}}{\text{Minimize}} \quad \sum_{b\in\mathcal{N}^{subs}}\left(C_b^{tr}p_b^{tr}\right) + \sum_{b\in\mathcal{N}}\Big(C^{ll,p+}\Delta D_b^{p+} + C^{ll,p-}\Delta D_b^{p-} + C^{ll,q+}\Delta D_b^{q+} + C^{ll,q-}\Delta D_b^{q-}\Big) + \sum_{l\in\mathcal{L}^{sw}}\left(C_l^{sw}y_l^{sw}\right) + \sup_{\mathcal{Q}\in\mathcal{P}(\boldsymbol{f}^p,\boldsymbol{\beta})}\mathbb{E}_{\mathcal{Q}}\Big[H\big(\boldsymbol{z}^{sw},\boldsymbol{a}^L\big)\Big] \quad (1)$$

subject to:

$$p_b^{tr} + \sum_{l\in\mathcal{L}|to(l)=b} f_l^p - \sum_{l\in\mathcal{L}|fr(l)=b} f_l^p - D_b^p - \Delta D_b^{p+} + \Delta D_b^{p-} = 0; \forall b\in\mathcal{N}^{subs} \quad (2)$$

$$q_b^{tr} + \sum_{l\in\mathcal{L}|to(l)=b} f_l^q - \sum_{l\in\mathcal{L}|fr(l)=b} f_l^q - \tan(\arccos(PF_b))D_b^p - \Delta D_b^{q+} + \Delta D_b^{q-} = 0; \forall b\in\mathcal{N}^{subs} \quad (3)$$

$$\sum_{l\in\mathcal{L}|to(l)=b} f_l^p - \sum_{l\in\mathcal{L}|fr(l)=b} f_l^p - D_b^p - \Delta D_b^{p+} + \Delta D_b^{p-} = 0; \forall b\in\mathcal{N}\setminus\mathcal{N}^{subs} \quad (4)$$

$$\sum_{l\in\mathcal{L}|to(l)=b} f_l^q - \sum_{l\in\mathcal{L}|fr(l)=b} f_l^q - \tan(\arccos(PF_b))D_b^p - \Delta D_b^{q+} + \Delta D_b^{q-} = 0; \forall b\in\mathcal{N}\setminus\mathcal{N}^{subs} \quad (5)$$

$$-v_{fr(l)}^{\dagger} + v_{to(l)}^{\dagger} + 2(R_l f_l^p + X_l f_l^q) - (1-z_l^{sw})M \le 0; \forall l\in\mathcal{L}^{sw} \quad (6)$$

$$v_{fr(l)}^{\dagger} - v_{to(l)}^{\dagger} - 2(R_l f_l^p + X_l f_l^q) - (1-z_l^{sw})M \le 0; \forall l\in\mathcal{L}^{sw} \quad (7)$$

$$v_{fr(l)}^{\dagger} - v_{to(l)}^{\dagger} - 2(R_l f_l^p + X_l f_l^q) = 0; \forall l\in\mathcal{L}\setminus\mathcal{L}^{sw} \quad (8)$$

$$\underline{V}_b^2 \le v_b^{\dagger} \le \overline{V}_b^2; \forall b\in\mathcal{N} \quad (9)$$

$$v_b^{\dagger} = V^{ref^2}; \forall b\in\mathcal{N}^{subs} \quad (10)$$

$$-z_l^{sw}\overline{F}_l \le f_l^p \le z_l^{sw}\overline{F}_l; \forall l\in\mathcal{L}^{sw} \quad (11)$$

$$-z_l^{sw}\overline{F}_l \le f_l^q \le z_l^{sw}\overline{F}_l; \forall l\in\mathcal{L}^{sw} \quad (12)$$

$$-\overline{F}_l \le f_l^p \le \overline{F}_l; \forall l\in\mathcal{L} \quad (13)$$

$$-\overline{F}_l \le f_l^q \le \overline{F}_l; \forall l\in\mathcal{L} \quad (14)$$

$$f_l^q - \cot\Big(\Big(\frac{1}{2}-e\Big)\frac{\pi}{4}\Big)\Big(f_l^p - \cos\Big(e\frac{\pi}{4}\Big)\overline{F}_l\Big) - \sin\Big(e\frac{\pi}{4}\Big)\overline{F}_l \le 0; \forall l\in\mathcal{L}, e\in\{1,\dots,4\} \quad (15)$$

$$-f_l^q - \cot\Big(\Big(\frac{1}{2}-e\Big)\frac{\pi}{4}\Big)\Big(f_l^p - \cos\Big(e\frac{\pi}{4}\Big)\overline{F}_l\Big) - \sin\Big(e\frac{\pi}{4}\Big)\overline{F}_l \le 0; \forall l\in\mathcal{L}, e\in\{1,\dots,4\} \quad (16)$$

$$0 \le p_b^{tr} \le \overline{P}_b^{tr}; \forall b\in\mathcal{N}^{subs} \quad (17)$$

$$\underline{Q}_b^{tr} \le q_b^{tr} \le \overline{Q}_b^{tr}; \forall b\in\mathcal{N}^{subs} \quad (18)$$

$$\Delta D_b^{p+}, \Delta D_b^{p-}, \Delta D_b^{q+}, \Delta D_b^{q-} \ge 0; \forall b\in\mathcal{N} \quad (19)$$

$$\Delta D_b^{p^-} \le D_b^p; \forall b\in\mathcal{N} \quad (20)$$

$$\Delta D_b^{q^-} \le \tan(\arccos(PF_b))(D_b^p); \forall b\in\mathcal{N} \quad (21)$$

$$y_l^{sw} \ge z_l^{sw} - z_l^{sw,0}; \forall l\in\mathcal{L}^{sw} \quad (22)$$

$$y_l^{sw} \ge z_l^{sw,0} - z_l^{sw}; \forall l\in\mathcal{L}^{sw} \quad (23)$$

$$\sum_{l\in\mathcal{L}_k^{forbid}} z_l^{sw} \le \Big|\mathcal{L}_k^{forbid}\Big| - 1; \forall k\in\mathcal{K}^{forbid} \quad (24)$$

$$z_l^{sw} \in \{0,1\}; \forall l\in\mathcal{L}^{sw}, \quad (25)$$

where sets $\mathcal{L}$, $\mathcal{L}^{sw}$, $\mathcal{K}^{forbid}$, $\mathcal{N}$, and $\mathcal{N}^{subs}$ contain indices of all line segments, line segments that can be switched on/off, line segments that cannot be simultaneously switched on (due to radiality constraints), all buses of the distribution system, and buses with substations, respectively. In addition, parameters C_b^{tr}, $C^{ll,p+}$, $C^{ll,p-}$, $C^{ll,q+}$, $C^{ll,q-}$, C_l^{sw}, $z_l^{sw,0}$, D_b^p, PF_b, V^{ref}, R_l, X_l, $\underline{V}_b$, $\overline{V}_b$, $\overline{F}_l$, $\overline{P}_b^{tr}$, $\overline{Q}_b^{tr}$, $\underline{Q}_b^{tr}$ represent cost of purchasing active power from the main transmission grid, cost of active power surplus, cost of active power loss, cost of reactive power surplus, cost of reactive power loss, cost of switching, initial switching status of switchable line segments (equal to 1 if switched on, 0 otherwise), active power demand, power factor, voltage reference, resistance, reactance, voltage lower bound, voltage upper bound, maximum power flow in each line segment, maximum active power injection at the substations, maximum reactive power injection at the substations, and minimum reactive power injection at the substations, respectively. Moreover, decision variables p_b^{tr}, q_b^{tr}, $v_b^{\dagger}$, f_l^p, f_l^q, y_l^{sw}, z_l^{sw}, ΔD_b^{p+}, ΔD_b^{p-}, ΔD_b^{q+}, ΔD_b^{q-} represent active power injected at the substations, reactive power injected at the substations, squared voltage, active power flow, reactive power flow, an indication of a switching action (equal to 1 if a switching action is scheduled, 0 otherwise), switching status, active power surplus, active power loss, reactive power surplus, and reactive power loss, respectively.

The main contribution of this paper is to propose a decision-making methodology that effectively captures decision-dependent uncertainty while operating distribution systems amidst wildfire-prone conditions. In addition to that, we also consider that the probability distributions of these failure probabilities are uncertain. Hence, we propose a distributionally robust optimization model that handles decision-dependent

uncertainty, which entails not only that probabilities of failure are not precisely known but also that they are affected by decisions. In order to consider these aspects, our formulation (1)–(25) includes, in the objective function, a term that represents the worst-case expectation of the second-stage operational cost. This worst-case expectation is modeled over all probability distributions within the set $\mathcal{P}(\boldsymbol{f}^p, \boldsymbol{\beta})$, which depends on the scheduled power flows ($\boldsymbol{f}^p$) and the (contextual) factors ($\boldsymbol{\beta}$). To enable the representation of decision-dependent uncertainty in a distributionally robust optimization model, we later define set $\mathcal{P}(\boldsymbol{f}^p, \boldsymbol{\beta})$ in expression (51) by considering that the upper bounds of failure probabilities are affine functions of the scheduled power flows. Based on this tailored definition of set $\mathcal{P}(\boldsymbol{f}^p, \boldsymbol{\beta})$, we reformulate and decompose problem (1)–(25) to propose a bespoke procedure (further discussed in Section III) that yields an optimal solution to the original problem, which is also an important contribution of this paper.

Problem (1)–(25) is a two-stage, mixed-integer, distributionally robust optimization problem with decision-dependent uncertainty (ambiguity set). The objective function (1) aims at minimizing a combination of active power injection purchases at the nodes with substations, loss of load costs, switching action, as well as the decision-dependent expected second-stage operational cost. More specifically, the latter is represented by $H(\mathbf{z}^{sw}, \boldsymbol{a}^L)$, a function of the first-stage switching decision ($\mathbf{z}^{sw}$) and the random vector $\boldsymbol{a}^L$ associated with the availability of line segments of the feeder. To do so, note that in (1), we formulate the ambiguity set $\mathcal{P}$ (that accounts for the collection of credible probability distributions of line availability uncertainty - this set will be better defined in Subsection II-A) as a function of the scheduled power flow ($\boldsymbol{f}^p$) and the (contextual) factors ($\boldsymbol{\beta}$) (also better defined in Subsection II-A) to characterize endogenous and exogenous influence to uncertainty in line failures, respectively.

Active and reactive power balance are modeled through constraints (2) and (3) for substations and via constraints (4) and (5) for the remaining buses. Constraints (6) and (7) model voltage difference between sending and receiving ends of switchable line segments, with M denoting a large number to relax these constraints when line $l \in \mathcal{L}^{sw}$ is switched off. Analogously, constraints (8) represent voltage drop for non-switchable line segments. Constraints (9) enforce voltage limits. Constraints (10) set the voltage at the substations equal to the voltage reference. Active power flows limits are imposed by constraints (11) for switchable line segments and by (13) for the remaining ones. Likewise, constraints (12) and (14) impose limits to reactive power flows, which are also limited according to current active power flows by constraints (15) and (16) similarly to the linearized AC power flow presented in [37]. Constraints (17) and (18) enforce limits on active and reactive power injections at the substations, respectively. Constraints (19) enforce non-negativity to power surplus and load shedding variables while constraints (20) and (21) impose upper limits on the load shedding variables at each node of the system. Such upper-limit levels are set as the total (active/reactive) demand of the respective node. Thus, the maximum power, which can be shed at each node by the system operator prescribed by the proposed distribution system operation model, is upper-bounded by the respective active and reactive demand. This constraint ensures alignment between the mathematical formulation and the actual implementation of the prescribed solution. Constraints (22) and (23) model the behavior of variable y_l^{sw}, which assumes value equal to 1 if the determined switching status z_l^{sw} of line segment $l \in \mathcal{L}^{sw}$ is different from its initial switching status $z_l^{sw,0}$. Constraints (24) model the forbidden switching patterns with $\mathcal{L}_k^{forbid}$ indicating the line segments that cannot be simultaneously switched on for each $k \in \mathcal{K}^{forbid}$. In practice, this set of rules is usually defined a priori by the operator to impose radiality constraints. Finally, constraints (25) impose the binary nature of the switching variables.

Following the decision-making process, the post-contingency operational problem is formulated in (26)–(47):

$$H(\boldsymbol{z}^{sw}, \boldsymbol{a}^L) = \underset{\substack{\Delta D_b^{p+^c}, \Delta D_b^{p-^c}, \\ \Delta D_b^{q+^c}, \Delta D_b^{q-^c}, \\ f_l^{p^c}, f_l^{q^c}, p_b^{tr^c}, q_b^{tr^c}, v_b^{\dagger^c}}}{\text{Minimize}} \sum_{b \in \mathcal{N}^{subs}} \left(C_b^{tr} p_b^{tr^c} \right) + \sum_{b \in \mathcal{N}} \Big(C^{ll,p+} \Delta D_b^{p+^c} + C^{ll,p-} \Delta D_b^{p-^c} + C^{ll,q+} \Delta D_b^{q+^c} + C^{ll,q-} \Delta D_b^{q-^c} \Big) \quad (26)$$

subject to:

$$p_b^{tr^c} + \sum_{l \in \mathcal{L} | to(l)=b} f_l^{p^c} - \sum_{l \in \mathcal{L} | fr(l)=b} f_l^{p^c} - D_b^p - \Delta D_b^{p+^c} + \Delta D_b^{p-^c} = 0 : (\eta_b^1); \forall b \in \mathcal{N}^{subs} \quad (27)$$

$$q_b^{tr^c} + \sum_{l \in \mathcal{L} | to(l)=b} f_l^{q^c} - \sum_{l \in \mathcal{L} | fr(l)=b} f_l^{q^c} - \tan(\arccos(PF_b)) D_b^p - \Delta D_b^{q+^c} + \Delta D_b^{q-^c} = 0 : (\eta_b^2); \forall b \in \mathcal{N}^{subs} \quad (28)$$

$$\sum_{l \in \mathcal{L} | to(l)=b} f_l^{p^c} - \sum_{l \in \mathcal{L} | fr(l)=b} f_l^{p^c} - D_b^p - \Delta D_b^{p+^c} + \Delta D_b^{p-^c} = 0 : (\eta_b^3); \forall b \in \mathcal{N} \setminus \mathcal{N}^{subs} \quad (29)$$

$$\sum_{l \in \mathcal{L} | to(l)=b} f^{q^c} - \sum_{l \in \mathcal{L} | fr(l)=b} f_l^{q^c} - \tan(\arccos(PF_b)) D_b^p - \Delta D_b^{q+^c} + \Delta D_b^{q-^c} = 0 : (\eta_b^4); \forall b \in \mathcal{N} \setminus \mathcal{N}^{subs} \quad (30)$$

$$- v_{fr(l)}^{\dagger^c} + v_{to(l)}^{\dagger^c} + 2(R_l f_l^{p^c} + X_l f_l^{q^c}) - (1 - a_l^L)M - (1 - z_l^{sw})M \leq 0 : (\eta_l^5); \forall l \in \mathcal{L}^{sw} \quad (31)$$

$$v_{fr(l)}^{\dagger^c} - v_{to(l)}^{\dagger^c} - 2(R_l f_l^{p^c} + X_l f_l^{q^c}) - (1 - a_l^L)M - (1 - z_l^{sw})M \leq 0 : (\eta_l^6); \forall l \in \mathcal{L}^{sw} \quad (32)$$

$$- v_{fr(l)}^{\dagger^c} + v_{to(l)}^{\dagger^c} + 2(R_l f_l^{p^c} + X_l f_l^{q^c}) - (1 - a_l^L)M \leq 0 : (\eta_l^7); \forall l \in \mathcal{L} \setminus \mathcal{L}^{sw} \quad (33)$$

$$v_{fr(l)}^{\dagger^c} - v_{to(l)}^{\dagger^c} - 2(R_l f_l^{p^c} + X_l f_l^{q^c}) - (1 - a_l^L)M \leq 0 : (\eta_l^8); \forall l \in \mathcal{L} \setminus \mathcal{L}^{sw} \quad (34)$$

$$\underline{V}_b^2 \leq v_b^{\dagger^c} \leq \overline{V}_b^2 : (\eta_b^9, \eta_b^{10}); \forall b \in \mathcal{N} \quad (35)$$

$$- z_l^{sw} \overline{F}_l \leq f_l^{p^c} \leq z_l^{sw} \overline{F}_l : (\eta_l^{11}, \eta_l^{12}); \forall l \in \mathcal{L}^{sw} \quad (36)$$

$$- z_l^{sw} \overline{F}_l \leq f_l^{q^c} \leq z_l^{sw} \overline{F}_l : (\eta_l^{13}, \eta_l^{14}); \forall l \in \mathcal{L}^{sw} \quad (37)$$

$$- a_l^L \overline{F}_l \leq f_l^{p^c} \leq a_l^L \overline{F}_l : (\eta_l^{15}, \eta_l^{16}); \forall l \in \mathcal{L} \quad (38)$$

$$- a_l^L \overline{F}_l \leq f_l^{q^c} \leq a_l^L \overline{F}_l : (\eta_l^{17}, \eta_l^{18}); \forall l \in \mathcal{L} \quad (39)$$

$$f_l^{q^c} - \cot\Big(\Big(\frac{1}{2} - e\Big)\frac{\pi}{4}\Big)\Big(f_l^{p^c} - \cos\Big(e\frac{\pi}{4}\Big)\overline{F}_l\Big)$$

$$-\sin\Big(e\frac{\pi}{4}\Big)\overline{F}_l \leq 0 : (\eta^{19}_{l,e}); \forall l \in \mathcal{L}, e \in \{1,\ldots,4\} \quad (40)$$

$$-f^{q^c}_l - \cot\Big(\Big(\frac{1}{2}-e\Big)\frac{\pi}{4}\Big)\Big(f^{p^c}_l - \cos\Big(e\frac{\pi}{4}\Big)\overline{F}_l\Big) - \sin\Big(e\frac{\pi}{4}\Big)\overline{F}_l \leq 0 : (\eta^{20}_{l,e}); \forall l \in \mathcal{L}, e \in \{1,\ldots,4\} \quad (41)$$

$$0 \leq p^{tr^c}_b \leq \overline{P}^{tr}_b : (\eta^{21}_b, \eta^{22}_b); \forall b \in \mathcal{N}^{subs} \quad (42)$$

$$\underline{Q}^{tr}_b \leq q^{tr^c}_b \leq \overline{Q}^{tr}_b : (\eta^{23}_b, \eta^{24}_b); \forall b \in \mathcal{N}^{subs} \quad (43)$$

$$v^{\dagger^c}_b = V^{ref^2} : (\eta^{25}_b); \forall b \in \mathcal{N}^{subs} \quad (44)$$

$$\Delta D^{p^{+^c}}_b, \Delta D^{p^{-^c}}_b, \Delta D^{q^{+^c}}_b, \Delta D^{q^{-^c}}_b \geq 0 : (\eta^{26}_b, \eta^{27}_b, \eta^{28}_b, \eta^{29}_b); \forall b \in \mathcal{N} \quad (45)$$

$$\Delta D^{p^{-^c}}_b \leq D^p_b : (\eta^{30}_b); \forall b \in \mathcal{N} \quad (46)$$

$$\Delta D^{q^{-^c}}_b \leq \tan(\arccos(PF_b))D^p_b : (\eta^{31}_b); \forall b \in \mathcal{N}, \quad (47)$$

where the symbols within parenthesis are the dual variables associated with the constraints. Problem (26)–(47) is a linear programming problem with (continuous) decision variables $p^{tr^c}_b$, $q^{tr^c}_b$, $v^{\dagger^c}_b$, $f^{p^c}_l$, $f^{q^c}_l$, $\Delta D^{p^{+^c}}_b$, $\Delta D^{p^{-^c}}_b$, $\Delta D^{q^{+^c}}_b$, and $\Delta D^{q^{-^c}}_b$ with essentially the same role as in (1)–(25). For didactic purposes, the decision variables of the problem (26)–(47) are presented with a superscript c to differentiate them from the ones with an analogous symbol in the first-stage problem (1)–(25). For instance, p^{tr}_b (decision variable of the first-stage problem) means the amount of active power injected at bus $b \in \mathcal{N}^{subs}$ at the first stage and the one with the superscript c, $p^{tr^c}_b$ (decision variable of the second-stage problem), has the same physical meaning (i.e., the amount of active power injected at bus $b \in \mathcal{N}^{subs}$), but prescribed for the second stage, hence for a given (known) contingency vector $\boldsymbol{a}^L$. Analogously to (2)–(5), constraints (27)–(30) model active and reactive power balances. Constraints (31)–(34) express voltage differences in line segments under a given contingency state associated with vector $\boldsymbol{a}^L$ and a first-stage switching decision z^{sw}_l. Constraints (35) impose voltage limits. Constraints (36)–(41) enforce limits to active and reactive flows. Constraints (42)–(47) limit power injections and impose voltage reference at the substations as well as enforce non-negativity to power surplus and power loss variables.

A. Decision-(Line-Flows)-Dependent Ambiguity Set Modeling

Following the discussion of the previous section, the proposed methodology for distribution system operations seeks for least-cost pre- and post-contingency states operative decisions, the latter with respect to line segment availability. We argue, furthermore, that such line availability is mainly influenced by exogenous weather conditions, in particular during adverse climate circumstances, as well as endogenously impacted by the determined operative point and power flow in the network [27]. To jointly tackle these two critical uncertain factors in a unified framework, in this section, a pre-contingency line-flow-dependent ambiguity set of credible branch availability probabilities is constructed. More specifically, the uncertainty related to the underlying stochastic process associated with line failures is modeled via a tailored ambiguity set $\mathcal{P} \in \mathcal{M}_+$ composed of a collection of probability distributions that characterize the limited knowledge of failure probabilities and the endogenous/exogenous uncertain impact factors. Formally, the proposed ambiguity set is expressed as:

$$\mathcal{P}(\boldsymbol{f}^p, \boldsymbol{\beta}) = \Big\{\mathcal{Q} \in \mathcal{M}_+(\mathcal{A}) \;\Big|\; \mathbb{E}_{\mathcal{Q}}\big[\boldsymbol{S}\hat{\boldsymbol{a}}^L\big] \leq \overline{\boldsymbol{\mu}}(\boldsymbol{f}^p, \boldsymbol{\beta})\Big\}. \quad (48)$$

In (48), function $\overline{\boldsymbol{\mu}}(\cdot,\cdot)$ is a vector of means that defines the dependency of external factors and decisions variables. The term $\boldsymbol{S}$ is defined as an auxiliary matrix of coefficients, and $\hat{\boldsymbol{a}}^L = \mathbb{1} - \boldsymbol{a}^L$ indicates a random vector of *line unavailability* with set $\mathcal{A}$ characterizing its support. In this work, the support of the random vector $\boldsymbol{a}^L$, is defined as

$$\mathcal{A} = \Big\{\boldsymbol{a}^L \in \{0,1\}^{|\mathcal{L}|} \;\Big|\; \sum_{l\in\mathcal{L}} a^L_l \geq |\mathcal{L}| - K\Big\}, \quad (49)$$

with K indicating the number of simultaneous unavailable system components (line segments, in the context of this work) [38], [39]. In essence, (48) establishes the set of probability distributions that measure the likelihood of occurrence of all credible line-contingency states, whose precise definition is presented in (49). Expression (49) in its turn defines the collection of credible contingency states that correspond to an $|\mathcal{L}|-K$ criterion, i.e., all network system states where at most K lines out of the available $|\mathcal{L}|$ lines can be out-of-service. Following the ambiguity set definition (48), fundamentally, a critical modeling element is the appropriate definition of the vector of means $\overline{\boldsymbol{\mu}}(\boldsymbol{f}^p, \boldsymbol{\beta})$. In this work, we follow the main findings in [27] and consider the following functional representation:

$$\overline{\boldsymbol{\mu}}(\boldsymbol{f}^p, \boldsymbol{\beta}) = \boldsymbol{\gamma} + \mathrm{diag}(\boldsymbol{\beta})|\boldsymbol{f}^p|, \quad (50)$$

where $\mathrm{diag}(\boldsymbol{\beta})$ returns a diagonal matrix with elements of $\boldsymbol{\beta}$. Structurally, vector $\boldsymbol{\gamma}$ represents an estimated upper bound for the nominal probability of failure associated with each line segment $l \in \mathcal{L}$, extracted from the set of available information (e.g., failures per year), whereas vector $\boldsymbol{\beta}$ (exogenous-impact) characterizes the sensitivity in the probability of failure to the scheduled active power flow (endogenous-impact) in each line. Within the context of this paper, on the one hand, vector $\boldsymbol{\beta}$ provides instrumental information on how the probability of line failure increases as a function of the power flows. On the other hand, in particular, during adverse climate conditions (e.g., dry weather and high wind speed), the line failure can be caused by fire, started by the line itself if it is sufficiently close to vegetation. This condition can be adjusted by the system operator using the contextual (exogenous) vector $\boldsymbol{\beta}$. Therefore, structurally, by setting $\boldsymbol{S} = \big[\mathbb{I} \mid -\mathbb{I}\big]^T_{2|\mathcal{L}|\times|\mathcal{L}|}$ and $\overline{\mu}_l = (\gamma_l + \beta_l|f^p_l|),\ \forall\ l \in \mathcal{L}$ and $\overline{\mu}_{(l+|\mathcal{L}|)} = 0,\ \forall\ l \in \mathcal{L}$ in (50), we have the resulting ambiguity set:

$$\mathcal{P}(\boldsymbol{f}^p, \boldsymbol{\beta}) = \Big\{\mathcal{Q} \in \mathcal{M}_+(\mathcal{A}) \;\Big|\; 0 \leq \mathbb{E}_{\mathcal{Q}}[\hat{a}^L_l] \leq \gamma_l + \beta_l|f^p_l|; \ \forall\ l \in \mathcal{L}\Big\}. \quad (51)$$

Since $\hat{\boldsymbol{a}}^L = \mathbb{1} - \boldsymbol{a}^L$ is a Bernoulli-type random vector, the structural specification of (51) implies that a failure probability in each line $l \in \mathcal{L}$ is constrained by the factor $\gamma_l + \beta_l|f^p_l|$, thus dependent on the (endogenous) scheduled active power flow f^p_l and the contextual (exogenous) information β_l. It is worth highlighting that the proposed distribution system operation model (1)–(25) with (51) has a decision process that follows a two-stage, distributionally robust optimization with decision-dependent ambiguity set rationale. This decision

process is formulated as a three-level system of optimization problems, not suitable for direct implementation on commercial solvers nor standard mathematical programming algorithms. Therefore, in the next section, we leverage the problem structure to devise a decomposition-based solution approach to efficiently handle the proposed model.

III. Solution methodology

The two-stage formulation (1)–(25) proposed in Section II is intended to model the operation of a distribution system while performing switching actions to minimize the worst-case expected cost in post-contingency operations. In this section, we develop an iterative procedure based on outer approximation to solve this problem. We begin by replacing the last term in (1) with α and writing (52). The variable α is defined through (54)–(56) which essentially represents the last term in (1). Thus, we equivalently rewrite model (1)–(25) as (52)–(56):

$$\begin{aligned}
&\underset{\substack{\alpha,\Delta D_b^{p+},\Delta D_b^{p-},\Delta D_b^{q+},\Delta D_b^{q-},\\ f_l^p,f_l^q,p_b^{tr},q_b^{tr},v_b^{\dagger},y_l^{sw},z_l^{sw}}}{\text{Minimize}} \quad \sum_{b\in\mathcal{N}^{subs}}\Big(C_b^{tr}p_b^{tr}\Big)\\
&\quad+\sum_{b\in\mathcal{N}}\Big(C^{ll,p+}\Delta D_b^{p+}+C^{ll,p-}\Delta D_b^{p-}\\
&\qquad+C^{ll,q+}\Delta D_b^{q+}+C^{ll,q-}\Delta D_b^{q-}\Big)\\
&\quad+\sum_{l\in\mathcal{L}^{sw}}\Big(C_l^{sw}y_l^{sw}\Big)+\alpha \qquad (52)\\
&\text{subject to:}\\
&\text{Constraints (2)–(25)} \qquad (53)\\
&\alpha=\Big\{\underset{\mathcal{Q}\in\mathcal{M}_+}{\text{Maximize}}\sum_{\boldsymbol{a}^L\in\mathcal{A}}H\big(\boldsymbol{z}^{sw},\boldsymbol{a}^L\big)\mathcal{Q}(\boldsymbol{a}^L) \qquad (54)\\
&\qquad\text{subject to:}\\
&\qquad\sum_{\boldsymbol{a}^L\in\mathcal{A}}\big(\boldsymbol{S}\hat{\boldsymbol{a}}^L\big)\mathcal{Q}(\boldsymbol{a}^L)\le\overline{\boldsymbol{\mu}}(\boldsymbol{f}^p,\boldsymbol{\beta}):(\boldsymbol{\psi}) \qquad (55)\\
&\qquad\sum_{\boldsymbol{a}^L\in\mathcal{A}}\mathcal{Q}(\boldsymbol{a}^L)=1 \qquad :(\varphi)\Big\}. \qquad (56)
\end{aligned}$$

Resorting to duality theory, we can substitute α in (52) by the dual objective function of the inner model (54)–(56) and replace (54)–(56) by the dual feasibility constraints (59). More precisely,

$$\begin{aligned}
&\underset{\substack{\Delta D_b^{p+},\Delta D_b^{p-},\Delta D_b^{q+},\Delta D_b^{q-},\varphi,\\ \boldsymbol{\psi}\ge\mathbf{0},f_l^p,f_l^q,p_b^{tr},q_b^{tr},v_b^{\dagger},y_l^{sw},z_l^{sw}}}{\text{Minimize}} \quad \sum_{b\in\mathcal{N}^{subs}}\Big(C_b^{tr}p_b^{tr}\Big)\\
&\quad+\sum_{b\in\mathcal{N}}\Big(C^{ll,p+}\Delta D_b^{p+}+C^{ll,p-}\Delta D_b^{p-}\\
&\qquad+C^{ll,q+}\Delta D_b^{q+}+C^{ll,q-}\Delta D_b^{q-}\Big)\\
&\quad+\sum_{l\in\mathcal{L}^{sw}}\Big(C_l^{sw}y_l^{sw}\Big)+\boldsymbol{\psi}^{\top}\overline{\boldsymbol{\mu}}(\boldsymbol{f}^p,\boldsymbol{\beta})+\varphi \qquad (57)\\
&\text{subject to:}\\
&\text{Constraints (2)–(25)} \qquad (58)\\
&\boldsymbol{\psi}^{\top}\boldsymbol{S}\hat{\boldsymbol{a}}^L+\varphi\ge H\big(\boldsymbol{z}^{sw},\boldsymbol{a}^L\big);\forall\ \boldsymbol{a}^L\in\mathcal{A}. \qquad (59)
\end{aligned}$$

To withstand the intractability caused by the combinatorial nature of the support set $\mathcal{A}$ defined in (49), we replace constraints in (59) by:

$$\varphi\ge\max_{\boldsymbol{a}^L\in\mathcal{A}}\Big\{H\big(\boldsymbol{z}^{sw},\boldsymbol{a}^L\big)-\boldsymbol{\psi}^{\top}\boldsymbol{S}\hat{\boldsymbol{a}}^L\Big\}. \qquad (60)$$

Based on (57), (58), (60), we propose in the next subsections an iterative procedure to address formulation (1)–(25).

A. Subproblem

The role of the subproblem is to provide an approximation to the right-hand side of (60). Note that $H(\boldsymbol{z}^{sw},\boldsymbol{a}^L)$ is a minimization problem. Thus, to build the subproblem, we take the following steps: (i) write the dual problem of $H(\boldsymbol{z}^{sw},\boldsymbol{a}^L)$, (ii) subtract the dual objective function by $\boldsymbol{\psi}^{\top}\boldsymbol{S}\hat{\boldsymbol{a}}^L$, and (iii) handle the bilinear products between dual and binary variables $\boldsymbol{a}^L$ in the dual objective function. It is worth mentioning that the recourse function associated with the resulting subproblem is convex with respect to the first-stage decision as it is a maximum of affine functions, therefore rendering the description of the right-hand side of (60) suitable to cutting planes approximation. The subproblem is fully provided in the Appendix.

B. Master problem

The master problem developed in this section is a relaxation of the original model (1)–(25). Such relaxation is improved by the iterative inclusion of cutting planes. The master problem is formulated as follows:

$$\begin{aligned}
&\underset{\substack{\Delta D_b^{p-},\Delta D_b^{p+},\Delta D_b^{q-},\Delta D_b^{q+},\\ \delta_{le},\xi_l,\rho_{le},\varphi,\chi_l,\boldsymbol{\psi}\ge\mathbf{0},f_l^p,\\ f_l^{p,-},f_l^{p,+},f_l^q,p_b^{tr},q_b^{tr},v_b^{\dagger},y_l^{sw},z_l^{sw}}}{\text{Minimize}} \quad \sum_{b\in\mathcal{N}^{subs}}\Big(C_b^{tr}p_b^{tr}\Big)\\
&\quad+\sum_{b\in\mathcal{N}}\Big(C^{ll,p+}\Delta D_b^{p+}+C^{ll,p-}\Delta D_b^{p-}\\
&\qquad+C^{ll,q+}\Delta D_b^{q+}+C^{ll,q-}\Delta D_b^{q-}\Big)\\
&\quad+\sum_{l\in\mathcal{L}^{sw}}\Big(C_l^{sw}y_l^{sw}\Big)+\sum_{l\in\mathcal{L}}\Big(\gamma_l\psi_l+\beta_l\chi_l\Big)+\varphi \qquad (61)\\
&\text{subject to:}\\
&\text{Constraints (2)–(25)} \qquad (62)\\
&f_l^p=f_l^{p,+}-f_l^{p,-};\forall l\in\mathcal{L} \qquad (63)\\
&0\le f_l^{p,+}\le\overline{F}_l\xi_l;\forall l\in\mathcal{L} \qquad (64)\\
&0\le f_l^{p,-}\le\overline{F}_l(1-\xi_l);\ \forall l\in\mathcal{L} \qquad (65)\\
&\xi_l\in\{0,1\};\forall l\in\mathcal{L} \qquad (66)\\
&f_l^{p,+}+f_l^{p,-}=s\sum_{e=1}^{E_l}2^{e-1}\delta_{le};\ \forall\ l\in\mathcal{L} \qquad (67)\\
&\delta_{le}\in\{0,1\};\forall l\in\mathcal{L},e\in1,\dots,E_l \qquad (68)\\
&-M(1-\delta_{le})\le\psi_l-\rho_{le}\le M(1-\delta_{le});\\
&\qquad\qquad\forall l\in\mathcal{L},e=1,\dots,E_l \qquad (69)\\
&-\delta_{le}M\le\rho_{le}\le\delta_{le}M;\ \forall l\in\mathcal{L},e=1,\dots,E_l \qquad (70)\\
&\chi_l=s\sum_{e=1}^{E_l}2^{e-1}\rho_{le};\forall l\in\mathcal{L} \qquad (71)\\
&\varphi\ge\sum_{b\in\mathcal{N}^{subs}}\Big[-D_b^p\eta_b^{1^{(j)}}-\tan\left(\arccos\left(PF_b\right)\right)D_b^p\eta_b^{2^{(j)}}\\
&\qquad+\underline{V}_b^2\eta_b^{9^{(j)}}-\overline{V}_b^2\eta_b^{10^{(j)}}-\overline{P}_b^{tr}\eta_b^{22^{(j)}}
\end{aligned}$$

$$
\begin{aligned}
&+ \underline{Q}_b^{tr}\eta_b^{23^{(j)}} - \overline{Q}_b^{tr}\eta_b^{24^{(j)}} - V^{ref^2}\eta_b^{25^{(j)}} \\
&- D_b^p\eta_b^{30^{(j)}} - \tan(\arccos(PF_b))D_b^p\eta_b^{31^{(j)}}\Big] \\
&+ \sum_{b\in\mathcal{N}\setminus\mathcal{N}^{subs}}\Big[-D_b^p\eta_b^{3^{(j)}} - \tan\left(\arccos\left(PF_b\right)\right)D_b^p\eta_b^{4^{(j)}} \\
&+ \underline{V}_b^2\eta_b^{9^{(j)}} - \overline{V}_b^2\eta_b^{10^{(j)}} \\
&- D_b^p\eta_b^{30^{(j)}} - \tan(\arccos(PF_b))D_b^p\eta_b^{31^{(j)}}\Big] \\
&+ \sum_{l\in\mathcal{L}\setminus\mathcal{L}^{sw}}\Big[-(1-a_l^{L^{(j)}})M\eta_l^{7^{(j)}} - (1-a_l^{L^{(j)}})M\eta_l^{8^{(j)}} \\
&- a_l^{L^{(j)}}\overline{F}_l\Big(\eta_l^{15^{(j)}} + \eta_l^{16^{(j)}} + \eta_l^{17^{(j)}} + \eta_l^{18^{(j)}}\Big) \\
&+ \sum_{e\in\{1,2,3,4\}}\Bigg(\overline{F}_l\Big[\cot\Big((\frac{1}{2}-e)\frac{\pi}{4}\Big)\cos\Big(e\frac{\pi}{4}\Big) \\
&- \sin\Big(e\frac{\pi}{4}\Big)\Big]\Big[\eta_{l,e}^{19^{(j)}} + \eta_{l,e}^{20^{(j)}}\Big]\Bigg)\Big] \\
&+ \sum_{l\in\mathcal{L}^{sw}}\Bigg[-\Big((1-a_l^{L^{(j)}})M + (1-z_l^{sw})M\Big)\eta_l^{5^{(j)}} \\
&- \Big((1-a_l^{L^{(j)}})M + (1-z_l^{sw})M\Big)\eta_l^{6^{(j)}} \\
&- z_l^{sw}\overline{F}_l\Big(\eta_l^{11^{(j)}} + \eta_l^{12^{(j)}} + \eta_l^{13^{(j)}} + \eta_l^{14^{(j)}}\Big) \\
&- a_l^{L^{(j)}}\overline{F}_l\Big(\eta_l^{15^{(j)}} + \eta_l^{16^{(j)}} + \eta_l^{17^{(j)}} + \eta_l^{18^{(j)}}\Big) \\
&+ \sum_{e\in\{1,2,3,4\}}\Bigg(\overline{F}_l\Big[\cot\Big((\frac{1}{2}-e)\frac{\pi}{4}\Big)\cos\Big(e\frac{\pi}{4}\Big) \\
&- \sin\Big(e\frac{\pi}{4}\Big)\Big]\Big[\eta_{l,e}^{19^{(j)}} + \eta_{l,e}^{20^{(j)}}\Big]\Bigg)\Bigg] \\
&- \sum_{l\in\mathcal{L}}\Big[\Big(\psi_l - \psi_{|\mathcal{L}|+l}\Big)\Big(1-a_l^{L^{(j)}}\Big)\Big]; \forall j\in\mathcal{J}, \qquad (72)
\end{aligned}
$$

where the product $\boldsymbol{\psi}^\top\overline{\boldsymbol{\mu}}(\boldsymbol{f}^p,\boldsymbol{\beta})$ in the objective function is replaced by $\sum_{l\in\mathcal{L}}(\gamma_l\psi_l+\beta_l\chi_l)$ and χ_l represents the bilinear term $\psi_l|f_l^p|$ as modeled in (63)–(71). More specifically, this set of constraints are derived by firstly modeling the absolute value of f_l^p, $\forall\, l\in\mathcal{L}$, through constraints (63)–(66) and discretizing this absolute value for each line segment in (67)–(68) using a binary expansion approach [40]. Then, the resulting binary-continuous bilinear products are linearized with the set of inequalities (69)–(70) following the McCormick envelopes technique [41]. Finally, variables χ_l are recovered in equations (71) by making use of the auxiliary variables ρ_{le} needed to construct the McCormick envelopes. Furthermore, expression (72) represents cutting planes that are iteratively included to approximate the right-hand side of expression (60).

C. Solution Algorithm

In this section, we describe the outer approximation algorithm proposed in this work, following the Master and Subproblem descriptions. Structurally, it is an iterative process that is carried out until the approximation provided by the inclusion of the cutting planes (72) is sufficient to make the solution of the relaxed Master problem close enough to optimality. This proposed outer approximation algorithm is summarized as follows.

1) Initialization: set counter $m \leftarrow 0$ and set $\mathcal{J} \leftarrow \emptyset$.
2) Solve the optimization model (61)–(72), store $\boldsymbol{z}^{sw(m)}$, $\boldsymbol{\psi}^{(m)}$ and $\varphi^{(m)}$, and set $LB^{(m)}$ equal to the value of the objective function (61).
3) Identify the worst-case contingency for $\boldsymbol{z}^{sw(m)}$ and $\boldsymbol{\psi}^{(m)}$ by running the linearized subproblem described in Subsection III-A. Store values of its decision variables and calculate $UB^{(m)}$ by subtracting $\varphi^{(m)}$ from $LB^{(m)}$ and adding the value of the objective function of the subproblem.
4) If $\big(UB^{(m)} - LB^{(m)}\big)/UB^{(m)} \leq \epsilon$, then STOP; else, CONTINUE.
5) Include in (61)–(72) a new cutting plane of the format (72) with decision variables stored in Step 3, set $m \leftarrow m+1$, $\mathcal{J} \leftarrow \mathcal{J}\cup\{m\}$, and go to Step 2.

It is interesting to note that the cuts generated when considering $\boldsymbol{\beta}=\mathbf{0}$ (i.e., neglecting decision-dependent uncertainty) are still valid for the decision-dependent case ($\boldsymbol{\beta}\geq\mathbf{0}$). This happens because the vectors of decision variables $\boldsymbol{z}^{sw}$ and $\boldsymbol{\psi}$ have the same feasible region regardless of the value of $\boldsymbol{\beta}$ and the cuts obtained by solving the maximization problem on the right-hand side of (60) would be valid even if $\boldsymbol{z}^{sw}$ and $\boldsymbol{\psi}$ are not optimally decided by the Master problem. In the numerical experiments conducted in this work, we will leverage this property to accelerate the solution of the cases with decision-dependent uncertainty ($\boldsymbol{\beta}\geq\mathbf{0}$) by reusing the cutting planes obtained for the case where decision-dependent uncertainty is not considered ($\boldsymbol{\beta}=\mathbf{0}$). This reuse can be particularly advantageous since: (i) it is usually much faster to solve the problem with $\boldsymbol{\beta}=\mathbf{0}$ and (ii) warming up the problem for $\boldsymbol{\beta}\geq\mathbf{0}$ with previously identified valid cutting planes can significantly improve computational efficiency as will be seen in the numerical experiments.

IV. Case Studies

The proposed methodology is illustrated in this section with two case studies. In both case studies, we consider that part of the grid is vulnerable to the ignition of a wildfire, which can be influenced by the levels of power flows passing through the line segments within the region. Furthermore, in both numerical experiments, we assume $K=1$ in (49) to characterize the support set $\mathcal{A}$. The first case study is based on a 54-bus distribution system, whereas the second one comprises a 138-bus distribution system. In both case studies, we consider that part of the grid is vulnerable to the ignition of a wildfire, which can be influenced by the levels of power flows passing through the line segments within the region. For replicability purposes, the input data can be downloaded from [42]. The solution algorithm described in Section III-C has been implemented in Julia 1.6 and solved on a server with one Intel® Core® i7-10700K processor @ 3.80GHz and 64 GB of RAM, using Gurobi 9.0.3. under JuMP.

A. 54-bus system

In this case, we consider a 54-bus distribution system (depicted in Fig. 2) based on the data provided in [43]. In this system, there are 3 substations (buses 51, 53, and 54 in Fig. 2) and 57 lines. The total demand of the system is 5400 kW and

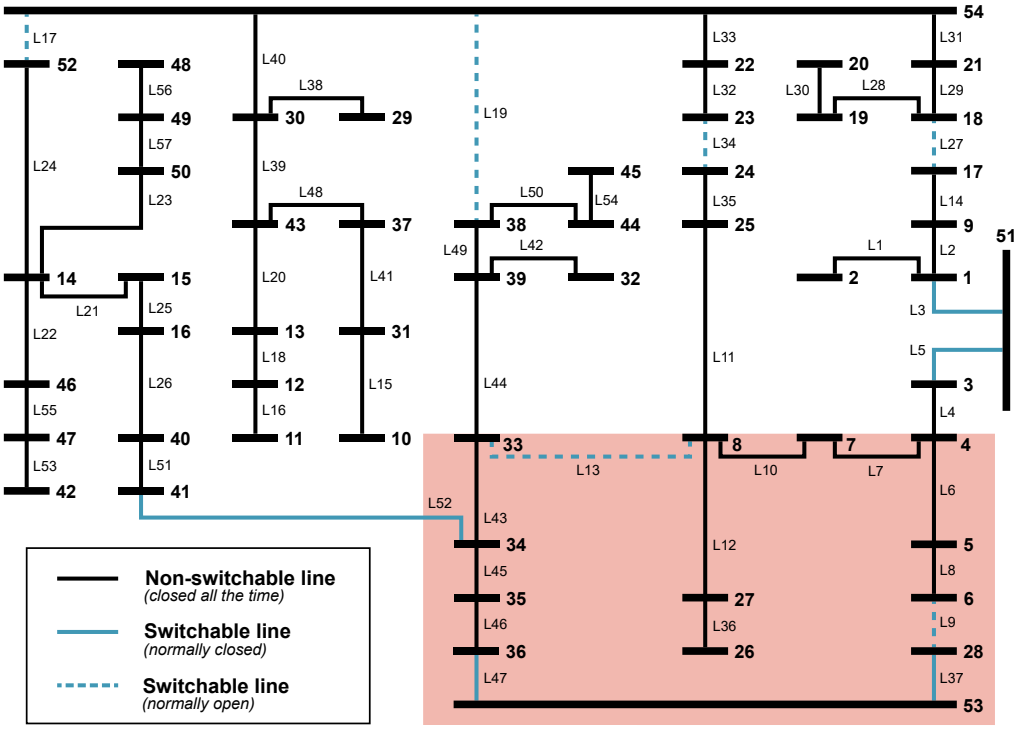

Fig. 2. 54-Bus distribution system.

the energy price is 0.01 $/kWh. In addition, we consider that each switching action costs $100, which can be performed in 11 out of the 57 lines. In Fig. 2, the switchable lines are represented by blue lines. Furthermore, the blue dashed lines are initially open lines whereas the blue solid lines are initially closed. To enforce radiality constraints, lines L9 and L37 cannot be switched on simultaneously. The same rule applies to the pairs of lines L17 and L52, L13 and L47, L5 and L34, L3 and L27, L13 and L19, L19 and L47, and L13 and L47. These rules constitute the forbidden switching patterns in this case study. In this case study, we consider an event of adverse climate conditions approaching that includes extreme dry weather and consistent wind speed. In addition, part of the grid, more specifically the southeast, is located close to vegetation, which renders this area particularly more likely to initiate a wildfire. The southeast area of the grid includes lines L6, L7, L8, L9, L10, L12, L13, L36, L37, L43, L45, L46, L47, and L52. We consider that every line segment has a nominal rate of failure equal to 0.4 failures per year. Using the exponential probability distribution, this rate of failure translates into a failure probability of 0.11% for each line in the next 24 hours. In addition, due to the adverse climate conditions, each of the aforementioned lines that belong to the southeast area has an increase of 3% in its probability of failure for each 0.01 pu (100kW) of scheduled active power flow. The remaining lines have an increase of 10^{-4}% in their probabilities of failure per 0.01 pu of scheduled active power flow.

We consider three possible modeling and algorithmic structures to determine the status of switchable lines. In the first one, hereinafter referred to as *without DDU* (Decision-Dependent Uncertainty), the operator ignores the decision-dependent influence of line flows and probabilities of failures in the modeling and, therefore, only considers the nominal probabilities previously described. To do so, equation (50) is modified to $\overline{\boldsymbol{\mu}} = \boldsymbol{\gamma}$. In the second one, hereinafter referred to as *with DDU*, the operator explicitly considers the aforementioned increase in failure probability corresponding to line usage according to (50). In the third one, hereinafter referred to as *with DDU and warm up*, decision-dependency is considered exactly as in the *with DDU* case but the cutting planes of the *without DDU* case are included in the master problem since the beginning of the execution of the solution algorithm. This reuse of cutting planes can help the *with DDU and warm up* approach to achieve the same solution of the *with DDU* method in less time. The respective switching statuses are depicted in Table I, where 1 means closed line and 0 means open line. As expected, when DDU is ignored, there is no incentive to change the status of any line since the nominal probabilities of failure are relatively low. Nonetheless, when DDU is considered, six lines have their statuses changed. In this context, the solution *without DDU* costs $54, which is equivalent to the cost of feeding the loads without any switching, and the solution *with DDU* costs $654, which includes feeding loads and performing 6 switching actions. The *with DDU and warm up* solution results in exactly the same costs and switching decisions as the

TABLE I
SWITCHING STATUS (1 FOR CLOSED AND 0 FOR OPEN LINES) WITH AND WITHOUT DDU

	Switchable Lines										
	3	**5**	**9**	**13**	**17**	**19**	**27**	**34**	**37**	**47**	**52**
W/out DDU	1	1	0	0	0	0	0	0	1	1	1
With DDU	1	0	0	0	1	1	0	1	1	0	0
With DDU and warm up	1	0	0	0	1	1	0	1	1	0	0

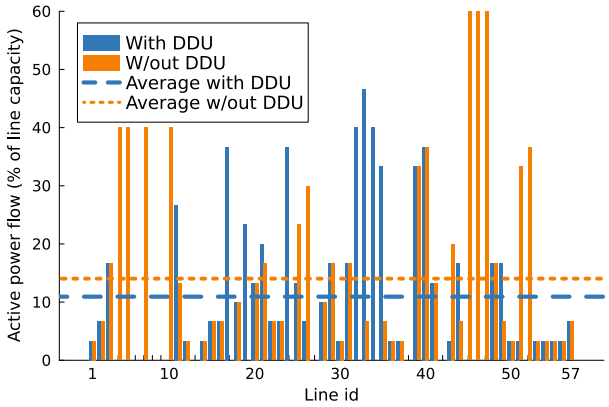

Fig. 3. Power flows for the solutions *with* and *without* DDU.

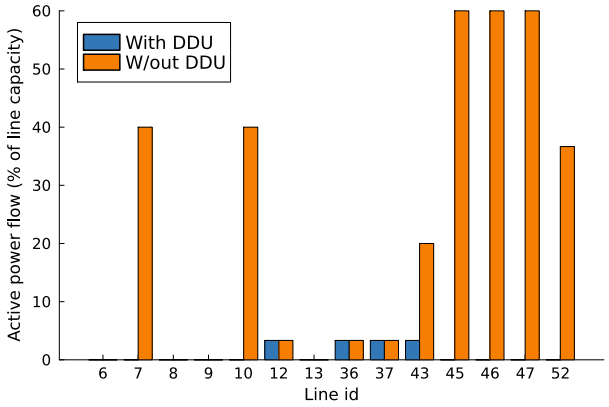

Fig. 4. 54-Bus system – Power flows through more vulnerable lines for the solutions *with* and *without DDU*.

with DDU solution. The solutions *without DDU*, *with DDU*, and *with DDU and warm up*, were obtained in 10.59s, 49.22s, and 22.50s, respectively.

In Fig. 3, it can be noted that the average flow per line, as well as the maximum flow among all branches, are significantly reduced when DDU is taken into account to decrease failure probabilities. This reduction occurs since, by recognizing that the power flows through the lines can increase failure probabilities, the proposed methodology decreases the average power flow level across all the line segments of the system under consideration while minimizing the system's loss of load. In addition, by considering the information about which line segments are closer to an area that is vulnerable to wildfires, the proposed methodology is able to strategically decrease power flow levels in this area, as illustrated in Fig. 4, and increase power flow levels in safer areas to compensate the demand supply.

1) Out-of-sample analysis: To compare the performance of both solutions provided in Table I, we conduct the following out-of-sample analysis. Firstly, we solve problem (1)–(25) forcing each of the two obtained switching decisions (without considering the last term in the objective function). Given the obtained power flows, we calculate the probability of failure for each line given switching decisions. Then, we generate 2000 scenarios of failure following a Bernoulli trial for the line states (1 in service; 0 failure) with the computed probabilities. Under these generated scenarios, we evaluate the performances of the two solutions. For this out-of-sample

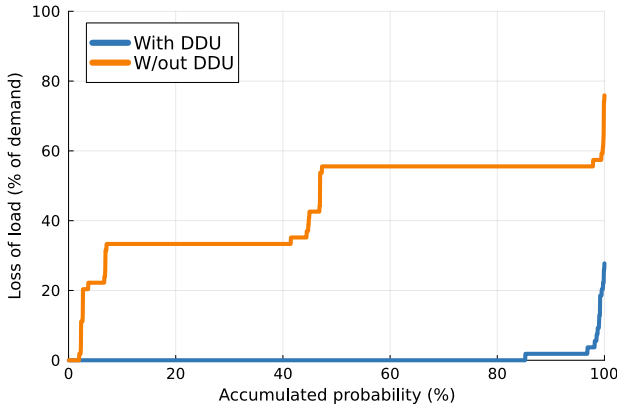

Fig. 5. Out-of-sample inverse cumulative distribution of the system loss of load for the solutions *with* and *without DDU*.

analysis, the average loss of load (% of total demand) for the solutions *without DDU* and *with DDU* are 44.15% and 0.53%, respectively. In addition, the $\text{CVaR}_{95\%}$ of loss of load (% of total demand) for the solutions *without DDU* and *with DDU* are 57.17% and 6.91%, respectively. Moreover, according to Fig. 5, the solution *with DDU* has 85.25% probability to incur in null loss of load and 96.85% probability to resulting in up to 2% of loss of load, whereas the solution *without DDU* has 98.00% probability to incur a loss of load and more than 90% probability to result in more than 30% of loss of load.

We note that the magnitude of the impact on loss of load probability is rooted in the topology reconfiguration prescribed by the two cases under analysis. More specifically, note from Table I that the cost-effective action prescribed under the *without DDU* case is to feed costumers using power mostly from substation Bus 53, by keeping lines L47 and L52 closed, i.e., no switching action is taken. Since the substation Bus 53 is at a wildfire-prone area, the likelihood of line failure closely linked to feeding part of the system with power coming from this feeding bus is high. This fact is due to the context and the relatively higher power flow needed to feed almost the whole system. Therefore, this topology reconfiguration potentially triggers the failure of important line segments, magnifying the system loss of load for several operating conditions (scenarios), inducing the observed high loss of load probability. It should be highlighted, nevertheless, that by appropriately taking into account wildfire-prone conditions when prescribing the topology reconfiguration (the *with DDU* case), the same performance metric was significantly improved for the same system and context conditions. In fact, the topology reconfiguration prescribed under the *with DDU* case is to feed costumers using power mostly from substation Bus 54, located in an area without critical wildfire conditions. This proposed reconfiguration is constituted by opening lines L5, L47, and L52 and closing lines L17, L19, and L34. Therefore, we argue that our proposed methodology can properly recognize the appropriate switching actions that are needed to significantly decrease the risk of loss of load within a decision-dependent uncertainty framework.

B. 138-bus system

We also consider the benefits and effectiveness of the proposed methodology in the larger and more complex 138-bus distribution system (Fig. 6), based on the data provided

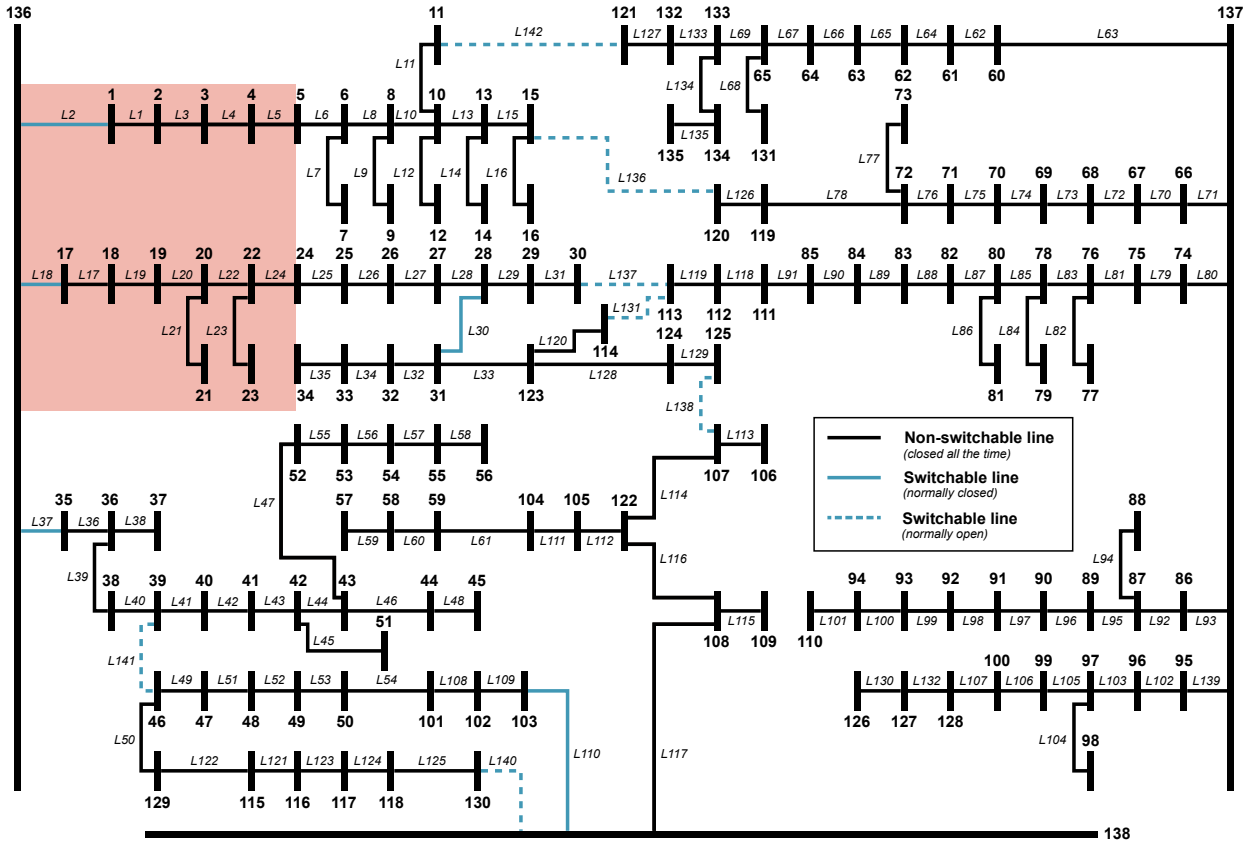

Fig. 6. 138-Bus distribution system.

in [43]. In this system, there are 3 substations, 138 buses, and 142 lines, from which 12 are switchable. The total demand of the system is 56,900 kW and the energy price is 0.2 $/kWh. We consider a penalty of 2 $/kWh for loss and surplus of both active and reactive power, and each switching action costs $200. To enforce radiality, we use a DFS (depth-first search) algorithm to identify 12 rules that avoid the simultaneous activation of line segments and result in the formation of cycles within the network. All branches have a nominal rate of failure equal to 0.15 per year and, analogously to Subsection IV-A, this rate of failure translates into a 0.0411% of failure probability (γ) for each line in the next 24 hours using the exponential probability distribution. Furthermore, the northwest part of the system is more likely to initiate a wildfire. This area of the grid includes lines L1–L5 and L17–L24.

In this numerical experiment, we conduct a sensitivity analysis of the impact of the β parameter in the solution by running the model *with DDU* 27 times, considering different values for β in the mentioned area. The range of the chosen values is defined considering the maximum failure probability ($\gamma + \beta\overline{F}$). This probability indicates how likely a line failure is to happen if the power flow in the feeder is at its maximum capacity. Given that, we choose β values for the lines in the wildfire area considering $\beta \times \overline{F}$ to range from 1% to 2% by 0.1%, from 2% to 10% by 1%, and from 10% to 90% by 10%. All the lines from outside the wildfire-prone area are assumed to have a $\beta \times \overline{F}$ as 0.1% in all cases.

The main results are depicted in Table II, where, for expository purposes, only the results for 8 cases are shown. These cases of maximum failure probability are important as they resulted in an operation change in terms of switching actions, for example, the cases between 1.1% and 1.8% resulted in the same switching decision, and so on. Besides that, values for the model *with DDU* refer to running the *with DDU and warm up* setup, since the warm-up helps in decreasing the computational burden to handle the decision-dependent model.

As depicted in Table II, as the value of β increases, the line risk of failure also increases, thus the solution is to change the grid by switching some critical lines. By changing the grid topology, the model decreases the power flow in the critical lines (inside the wildfire-prone area), decreasing the risk of failure associated with $\boldsymbol{\beta}$. Moreover, as we increase the level of $\boldsymbol{\beta}$, the worst-case expected value of post-contingency operation cost increases until it is worth performing switching actions. For instance, in the cases where only 4 lines are switched, between 1.9% and 3%, the worst-case expected value increases up to $12,565. At 4%, similarly, it is economically viable to afford further two switching actions and have a lower worst-case expected value. Therefore, as we increase the influence of the power flow levels through some line segment on their corresponding failure probabilities, the proposed methodology is able to recognize the impact and perform the appropriate switching actions, therefore yielding more risk-averse solutions. These switching actions are intended to decrease the power flows through the most vulnerable line

TABLE II
MAIN RESULTS - 138-BUS SYSTEM

	W/out DDU	With DDU							
Maximum failure probability	-	**1.0%**	**1.1%**	**1.8%**	**1.9%**	**3%**	**4%**	**50%**	**90%**
Switching actions (line index)	-	-	30; 138	30; 138	2; 30; 136; 138	2; 30; 136; 138	2; 18; 30; 136; 137; 138	2; 18; 30; 136; 137; 138	2; 18; 30; 136; 137; 138
Objective function value ($)	23,110	24,118	24,199	24,523	24,555	24,745	24,872	25,582	26,200
Energy	11,380	11,380	11,380	11,380	11,380	11,380	11,380	11,380	11,380
Switching	0	0	400	400	800	800	1,200	1,200	1,200
Deficit	0	0	0	0	0	0	0	0	0
Worst-case expected value of post-contingency operation cost	11,730	12,738	12,419	12,743	12,375	12,565	12,292	13,002	13,620
Computing time (min)	2.47	7.26	8.90	14.87	15.35	15.14	18.71	16.39	19.42

segments, which, as a consequence, results in dramatically lower metrics of average and $\text{CVaR}_{95\%}$ of loss of load as can be seen in our further discussed out-of-sample analysis with Fig. 7 and Fig. 8. These lower levels of loss of load can be translated into avoiding large costs for not serving the demand, which is an economic benefit of our methodology.

In general, the solution time of each case also increases with the $\boldsymbol{\beta}$ levels, reaching a maximum elapsed time of roughly 20 minutes. Essentially, when decision-dependent uncertainty is neglected ($\beta_l = 0,\ \forall\ l \in \mathcal{L}$), the impact of power flow levels on failure probabilities is not considered. Therefore, the switching decisions are the only first-stage decision variables to influence the outcome of the worst-case expected value of post-contingency costs, which is represented by the last term in the mathematical expression (1). With $\beta_l = 0$ for all lines, γ_l is the only remaining parameter in the line failure probability affine function, defined in expression (50). Since in our case studies, we consider γ_l as a low routine failure probability for all lines, different first-stage switching decisions lead to the same outcome of the worst-case expected value of post-contingency costs when $\beta_l = 0,\ \forall\ l \in \mathcal{L}$. The solution algorithm can then efficiently recognize that no switching decision would decrease the worst-case expected value of post-contingency costs and, since switching decisions have an associated cost, switching is not performed. It is worth mentioning that switching actions only take place when the decrease in the worst-case expected value of post-contingency costs offsets the switching costs. On the other hand, when we consider that power flow levels can impact line failure probabilities ($\beta_l \geq 0$, for any $l \in \mathcal{L}$), the solution algorithm needs more information from the subproblem to better describe in the master problem how the worst-case expected value of post-contingency costs could decrease depending on the first-stage switching actions. In this case, different combinations of switching actions can decrease the worst-case expected value of post-contingency costs. Consequently, the solution algorithm needs more iterations to determine the least-cost combination of switching actions that can lead to the highest decrease in the worst-case expected value of post-contingency costs. Moreover, the impact of power flow levels on line failure probabilities increases as we consider higher values of β_l, which prompts the solution algorithm to usually require more time to approximate the worst-case expected value of post-contingency costs so as to identify the optimal combination of switching actions.

1) Out-of-sample analysis: Finally, we also perform an out-of-sample analysis using the same procedure presented

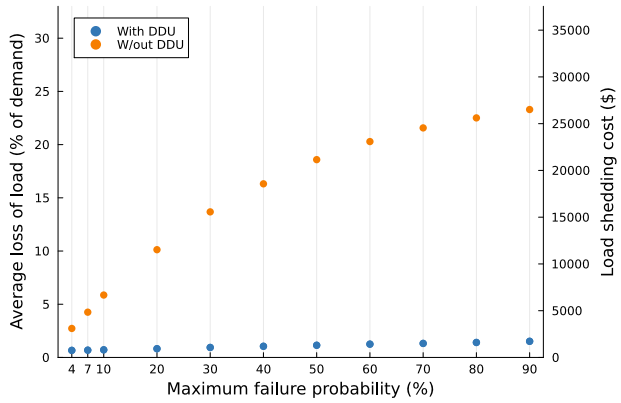

Fig. 7. Average loss of load (% total demand) in the out-of-sample analysis for the solution setup *with DDU* and *without DDU* for different levels of maximum failure probability.

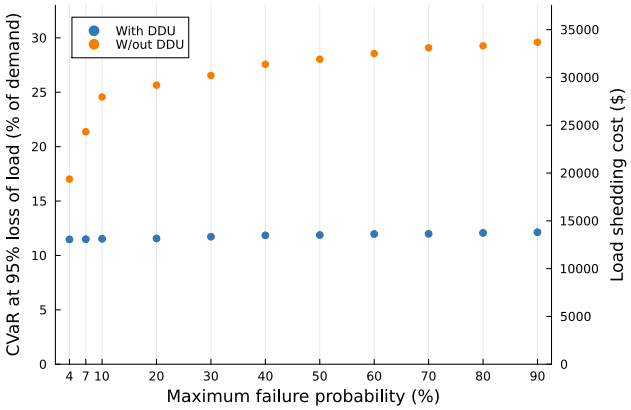

Fig. 8. $\text{CVaR}_{95\%}$ loss of load (% total demand) in the out-of-sample analysis for the solution setup *with DDU* and *without DDU* for different levels of maximum failure probability.

for the 54-bus system. In the 138-bus system, we consider the results of using each parameter $\boldsymbol{\beta}$. Firstly, in Fig. 7, we showcase the average load shedding for the out-of-sample analysis for each level of maximum failure probability ($\gamma + \beta\overline{F}$). Note that, as the environmental conditions for a wildfire worsen, the impact of the average loss of load when disregarding the DDU increases significantly. For instance, for a maximum failure probability of 90%, the average loss of load would be roughly 22% of total demand if no actions were considered (*without DDU*), while it would be roughly 1% if the actions suggested by the DDU model were implemented. Furthermore, Fig. 8 depicts a similar analysis, but highlighting the associated

$\text{CVaR}_{95\%}$ level. Note that, for the setup *without DDU*, a value of roughly 30% in loss of load (in % of total demand) can be observed in the most critical scenarios. On the other hand, nevertheless, the system topology prescribed by the *with DDU* setup significantly mitigates the load shedding occurrence and, consequently, the system operation cost. For instance, consider the maximum failure probability of 90% once more. The average cost in the *without DDU* setup is \$26,512 (Fig. 7), which is higher than the expected cost in the 5% worst-valued scenarios ($\text{CVaR}_{95\%}$), given by \$13,806, when prescribing the network topology based on the *with DDU* setup (Fig. 8).

V. Conclusion

This paper proposes a novel methodology to operate distribution systems amidst adverse climate conditions. We acknowledge that the likelihood of a line failure is dependent on its scheduled power flow and aggravated under a wildfire-prone environment. Therefore, in this work, we leverage a Decision-Dependent Uncertainty (DDU) framework to characterize the climate- and power-flow-dependent line availability probability function to devise a wildfire-aware distribution grid operation methodology and prescribe optimal switching actions to decrease the usage level of lines in peril locations, resulting in a more reliable operative condition. Two numerical experiments were conducted to illustrate the effectiveness of the proposed methodology. The results demonstrated that by properly considering DDU, our methodology can keep supplying loads when preventive switching actions are taken. This new configuration leads to a decrease in power flows near the areas where wildfire ignitions are more likely to occur. By doing that, the risk of failure and the risk of load loss are reduced. Although this method can be seen as a better alternative to PSPS, the model can also be adapted to determine where the shut-offs actions should be made.

Our framework has been built upon a linear representation of power flows through distribution grids while imposing radiality constraints. An extension to consider distribution systems operated as meshed networks and transmission systems is viable since the linear structure of the power flow constraints can be preserved and we will explore this possibility in future work. In addition, other interesting future research avenues are the inclusion of switching actions as recourse decisions and correlated cascading failures. While the former will require an approach to deal with a non-convex recourse problem, the latter will imply considering more statistical information in the definition of the decision-dependent ambiguity sets. Moreover, future research to optimally decide investments to upgrade existing line segments with switching devices and to install new line segments considering wildfire-prone conditions would be relevant to increase the flexibility of the system operators to deal with these events. Further case studies considering a sensitivity analysis depending on wind speeds, age, pole class, and type as well as improvement to capture the additional risk associated with having power flow levels higher than the rating of line segments will also constitute relevant next steps for this line of research.

Appendix

Following the steps described in Subsection III-A, the Subproblem model is written as:

$$
\begin{aligned}
\underset{\substack{a_l^L,\eta_b^{1\text{-}4},\eta_l^{5\text{-}8},\eta_b^{9\text{-}10},\eta_l^{11\text{-}18},\\ \eta_{l,e}^{19\text{-}20},\eta_b^{21\text{-}31},\lambda_l^{a\eta^{5\text{-}8}},\lambda_l^{a\eta^{15\text{-}18}}}}{\text{Maximize}} \quad & \sum_{b\in\mathcal{N}^{subs}}\Bigg(-D_b^p\eta_b^1 \\
& -\tan\Big(\arccos\left(PF_b\right)\Big)D_b^p\eta_b^2+\underline{V}_b^2\eta_b^9-\overline{V}_b^2\eta_b^{10} \\
& -\overline{P}_b^{tr}\eta_b^{22}+\underline{Q}_b^{tr}\eta_b^{23}-\overline{Q}_b^{tr}\eta_b^{24}-V^{ref^2}\eta_b^{25} \\
& -D_b^p\eta_b^{30}-\tan\Big(\arccos(PF_b)\Big)D_b^p\eta_b^{31}\Bigg) \\
+\sum_{b\in\mathcal{N}\setminus\mathcal{N}^{subs}}\Bigg(& -D_b^p\eta_b^3-\tan\Big(\arccos\left(PF_b\right)\Big)D_b^p\eta_b^4 \\
& +\underline{V}_b^2\eta_b^9-\overline{V}_b^2\eta_b^{10}-D_b^p\eta_b^{30} \\
& -\tan\Big(\arccos(PF_b)\Big)D_b^p\eta_b^{31}\Bigg) \\
+\sum_{l\in\mathcal{L}\setminus\mathcal{L}^{sw}}\Bigg(& -M\eta_l^7+M\lambda_l^{a\eta^7}-M\eta_l^8+M\lambda_l^{a\eta^8} \\
& -\overline{F}_l\Big(\lambda_l^{a\eta^{15}}+\lambda_l^{a\eta^{16}}+\lambda_l^{a\eta^{17}}+\lambda_l^{a\eta^{18}}\Big) \\
& +\sum_{e\in\{1,2,3,4\}}\Bigg[\overline{F}_l\Big(\cot\Big((\frac{1}{2}-e)(\frac{\pi}{4})\Big)\cos(e\frac{\pi}{4}) \\
& -\sin(e\frac{\pi}{4})\Big)\Big(\eta_{l,e}^{19}+\eta_{l,e}^{20}\Big)\Bigg]\Bigg) \\
+\sum_{l\in\mathcal{L}^{sw}}\Bigg(& -M\eta_l^5+M\lambda_l^{a\eta^5}-M\eta_l^5+Mz_l^{sw}\eta_l^5 \\
& -M\eta_l^6+M\lambda_l^{a\eta^6}-M\eta_l^6+Mz_l^{sw}\eta_l^6 \\
& -z_l^{sw}\overline{F}_l\Big(\eta_l^{11}+\eta_l^{12}+\eta_l^{13}+\eta_l^{14}\Big) \\
& -\overline{F}_l\Big(\lambda_l^{a\eta^{15}}+\lambda_l^{a\eta^{16}}+\lambda_l^{a\eta^{17}}+\lambda_l^{a\eta^{18}}\Big) \\
& +\sum_{e\in\{1,2,3,4\}}\Bigg[\overline{F}_l\Big(\cot\Big((\frac{1}{2}-e)(\frac{\pi}{4})\Big)\cos(e\frac{\pi}{4}) \\
& -\sin(e\frac{\pi}{4})\Big)\Big(\eta_{l,e}^{19}+\eta_{l,e}^{20}\Big)\Bigg]\Bigg) \\
-\sum_{l\in\mathcal{L}}\Bigg(& \Big(\psi_l-\psi_{|\mathcal{L}|+l}\Big)\Big(1-a_l^L\Big)\Bigg) \qquad (73)
\end{aligned}
$$

subject to:

$$C_b^{tr}+\eta_b^1-\eta_b^{21}+\eta_b^{22}=0:(p_b^{tr^c});\forall b\in\mathcal{N}^{subs} \qquad (74)$$

$$\eta_b^2-\eta_b^{23}+\eta_b^{24}=0:(q_b^{tr^c});\forall b\in\mathcal{N}^{subs} \qquad (75)$$

$$
\begin{aligned}
& \sum_{l\in\mathcal{L}^{sw}|b=fr(l)}\Big(\eta_l^6-\eta_l^5\Big)+\sum_{l\in\mathcal{L}^{sw}|b=to(l)}\Big(\eta_l^5-\eta_l^6\Big) \\
& +\sum_{l\in\mathcal{L}\setminus\mathcal{L}^{sw}|b=fr(l)}\Big(\eta_l^8-\eta_l^7\Big)+\sum_{l\in\mathcal{L}\setminus\mathcal{L}^{sw}|b=to(l)}\Big(\eta_l^7-\eta_l^8\Big) \\
& -\eta_b^9+\eta_b^{10}=0:(v_b^{\dagger^c});\forall b\in\mathcal{N}\setminus\mathcal{N}^{subs} \qquad (76) \\
& \sum_{l\in\mathcal{L}^{sw}|b=fr(l)}\Big(\eta_l^6-\eta_l^5\Big)+\sum_{l\in\mathcal{L}^{sw}|b=to(l)}\Big(\eta_l^5-\eta_l^6\Big) \\
& +\sum_{l\in\mathcal{L}\setminus\mathcal{L}^{sw}|b=fr(l)}\Big(\eta_l^8-\eta_l^7\Big)+\sum_{l\in\mathcal{L}\setminus\mathcal{L}^{sw}|b=to(l)}\Big(\eta_l^7-\eta_l^8\Big)
\end{aligned}
$$

$$-\eta_b^9+\eta_b^{10}+\eta_b^{25}=0:(v_b^{\dagger^c});\forall b\in\mathcal{N}^{subs} \quad (77)$$

$$\sum_{b\in\mathcal{N}^{subs}|b=to(l)}\eta_b^1-\sum_{b\in\mathcal{N}^{subs}|b=fr(l)}\eta_b^1+\sum_{b\in\mathcal{N}\setminus\mathcal{N}^{subs}|b=to(l)}\eta_b^3-\sum_{b\in\mathcal{N}\setminus\mathcal{N}^{subs}|b=fr(l)}\eta_b^3+2R_l\eta_l^7-2R_l\eta_l^8-\eta_l^{15}+\eta_l^{16}+\sum_{e\in\{1,2,3,4\}}\left[-\cot\Big((\frac{1}{2}-e)(\frac{\pi}{4})\Big)\Big(\eta_{l,e}^{19}\Big)-\cot\Big((\frac{1}{2}-e)(\frac{\pi}{4})\Big)\Big(\eta_{l,e}^{20}\Big)\right]=0:(f_l^{p^c});\forall l\in\mathcal{L}\setminus\mathcal{L}^{sw} \quad (78)$$

$$\sum_{b\in\mathcal{N}^{subs}|b=to(l)}\eta_b^1-\sum_{b\in\mathcal{N}^{subs}|b=fr(l)}\eta_b^1+\sum_{b\in\mathcal{N}\setminus\mathcal{N}^{subs}|b=to(l)}\eta_b^3-\sum_{b\in\mathcal{N}\setminus\mathcal{N}^{subs}|b=fr(l)}\eta_b^3+2R_l\eta_l^5-2R_l\eta_l^6-\eta_l^{11}+\eta_l^{12}-\eta_l^{15}+\eta_l^{16}+\sum_{e\in\{1,2,3,4\}}\left[-\cot\Big((\frac{1}{2}-e)(\frac{\pi}{4})\Big)\Big(\eta_{l,e}^{19}\Big)-\cot\Big((\frac{1}{2}-e)(\frac{\pi}{4})\Big)\Big(\eta_{l,e}^{20}\Big)\right]=0:(f_l^{p^c});\forall l\in\mathcal{L}^{sw} \quad (79)$$

$$\sum_{b\in\mathcal{N}^{subs}|b=to(l)}\eta_b^2-\sum_{b\in\mathcal{N}^{subs}|b=fr(l)}\eta_b^2+\sum_{b\in\mathcal{N}\setminus\mathcal{N}^{subs}|b=to(l)}\eta_b^4-\sum_{b\in\mathcal{N}\setminus\mathcal{N}^{subs}|b=fr(l)}\eta_b^4+2X_l\eta_l^7-2X_l\eta_l^8-\eta_l^{17}+\eta_l^{18}+\sum_{e\in\{1,2,3,4\}}\Big(\eta_{l,e}^{19}-\eta_{l,e}^{20}\Big)=0:(f_l^{q^c});\forall l\in\mathcal{L}\setminus\mathcal{L}^{sw} \quad (80)$$

$$\sum_{b\in\mathcal{N}^{subs}|b=to(l)}\eta_b^2-\sum_{b\in\mathcal{N}^{subs}|b=fr(l)}\eta_b^2+\sum_{b\in\mathcal{N}\setminus\mathcal{N}^{subs}|b=to(l)}\eta_b^4-\sum_{b\in\mathcal{N}\setminus\mathcal{N}^{subs}|b=fr(l)}\eta_b^4+2X_l\eta_l^5-2X_l\eta_l^6-\eta_l^{13}+\eta_l^{14}-\eta_l^{17}+\eta_l^{18}+\sum_{e\in\{1,2,3,4\}}\Big(\eta_{l,e}^{19}-\eta_{l,e}^{20}\Big)=0:(f_l^{q^c});\forall l\in\mathcal{L}^{sw} \quad (81)$$

$$C^{ll,p+}-\eta_b^3-\eta_b^{26}=0:(\Delta D_b^{p+^c});\forall b\in\mathcal{N}\setminus\mathcal{N}^{subs} \quad (82)$$

$$C^{ll,p+}-\eta_b^1-\eta_b^{26}=0:(\Delta D_b^{p+^c});\forall b\in\mathcal{N}^{subs} \quad (83)$$

$$C^{ll,p-}+\eta_b^3-\eta_b^{27}+\eta_b^{30}=0:(\Delta D_b^{p-^c});\forall b\in\mathcal{N}\setminus\mathcal{N}^{subs} \quad (84)$$

$$C^{ll,p-}+\eta_b^1-\eta_b^{27}+\eta_b^{30}=0:(\Delta D_b^{p-^c});\forall b\in\mathcal{N}^{subs} \quad (85)$$

$$C^{ll,q+}-\eta_b^4-\eta_b^{28}=0:(\Delta D_b^{q+^c});\forall b\in\mathcal{N}\setminus\mathcal{N}^{subs} \quad (86)$$

$$C^{ll,q+}-\eta_b^2-\eta_b^{28}=0:(\Delta D_b^{q+^c});\forall b\in\mathcal{N}^{subs} \quad (87)$$

$$C^{ll,q-}+\eta_b^4-\eta_b^{29}+\eta_b^{31}=0:(\Delta D_b^{q-^c});\forall b\in\mathcal{N}\setminus\mathcal{N}^{subs} \quad (88)$$

$$C^{ll,q-}+\eta_b^2-\eta_b^{29}+\eta_b^{31}=0:(\Delta D_b^{q-^c});\forall b\in\mathcal{N}^{subs} \quad (89)$$

$$-(1-a_l^L)M\le\eta_l^5-\lambda_l^{a\eta^5}\le(1-a_l^L)M;\forall l\in\mathcal{L}^{sw} \quad (90)$$

$$-(a_l^L)M\le\lambda_l^{a\eta^5}\le(a_l^L)M;\forall l\in\mathcal{L}^{sw} \quad (91)$$

$$-(1-a_l^L)M\le\eta_l^6-\lambda_l^{a\eta^6}\le(1-a_l^L)M;\forall l\in\mathcal{L}^{sw} \quad (92)$$

$$-(a_l^L)M\le\lambda_l^{a\eta^6}\le(a_l^L)M;\forall l\in\mathcal{L}^{sw} \quad (93)$$

$$-(1-a_l^L)M\le\eta_l^7-\lambda_l^{a\eta^7}\le(1-a_l^L)M;\ \forall l\in\mathcal{L}\setminus\mathcal{L}^{sw} \quad (94)$$

$$-(a_l^L)M\le\lambda_l^{a\eta^7}\le(a_l^L)M;\forall l\in\mathcal{L}\setminus\mathcal{L}^{sw} \quad (95)$$

$$-(1-a_l^L)M\le\eta_l^8-\lambda_l^{a\eta^8}\le(1-a_l^L)M;\ \forall l\in\mathcal{L}\setminus\mathcal{L}^{sw} \quad (96)$$

$$-(a_l^L)M\le\lambda_l^{a\eta^8}\le(a_l^L)M;\forall l\in\mathcal{L}\setminus\mathcal{L}^{sw} \quad (97)$$

$$-(1-a_l^L)M\le\eta_l^{15}-\lambda_l^{a\eta^{15}}\le(1-a_l^L)M;\forall l\in\mathcal{L} \quad (98)$$

$$-(a_l^L)M\le\lambda_l^{a\eta^{15}}\le(a_l^L)M;\forall l\in\mathcal{L} \quad (99)$$

$$-(1-a_l^L)M\le\eta_l^{16}-\lambda_l^{a\eta^{16}}\le(1-a_l^L)M;\forall l\in\mathcal{L} \quad (100)$$

$$-(a_l^L)M\le\lambda_l^{a\eta^{16}}\le(a_l^L)M;\forall l\in\mathcal{L} \quad (101)$$

$$-(1-a_l^L)M\le\eta_l^{17}-\lambda_l^{a\eta^{17}}\le(1-a_l^L)M;\forall l\in\mathcal{L} \quad (102)$$

$$-(a_l^L)M\le\lambda_l^{a\eta^{17}}\le(a_l^L)M;\forall l\in\mathcal{L} \quad (103)$$

$$-(1-a_l^L)M\le\eta_l^{18}-\lambda_l^{a\eta^{18}}\le(1-a_l^L)M;\forall l\in\mathcal{L} \quad (104)$$

$$-(a_l^L)M\le\lambda_l^{a\eta^{18}}\le(a_l^L)M;\forall l\in\mathcal{L} \quad (105)$$

$$\sum_{l\in\mathcal{L}}a_l^L\ge|\mathcal{L}|-K \quad (106)$$

$$\eta_b^1,\eta_b^2,\eta_b^{25}\in\mathbb{R};\forall b\in\mathcal{N}^{subs} \quad (107)$$

$$\eta_b^3,\eta_b^4\in\mathbb{R};\forall b\in\mathcal{N}\setminus\mathcal{N}^{subs} \quad (108)$$

$$\eta_b^9,\eta_b^{10},\eta_b^{26},\eta_b^{27},\eta_b^{28},\eta_b^{29},\eta_b^{30},\eta_b^{31}\ge0;\forall b\in\mathcal{N} \quad (109)$$

$$\eta_b^{21},\eta_b^{22},\eta_b^{23},\eta_b^{24}\ge0;\forall b\in\mathcal{N}^{subs} \quad (110)$$

$$\eta_l^{15},\eta_l^{16},\eta_l^{17},\eta_l^{18}\ge0;\forall l\in\mathcal{L} \quad (111)$$

$$\eta_{l,e}^{19},\eta_{l,e}^{20}\ge0;\forall l\in\mathcal{L},\forall e\in\{1,2,3,4\} \quad (112)$$

$$\eta_l^5,\eta_l^6,\eta_l^{11},\eta_l^{12},\eta_l^{13},\eta_l^{14}\ge0;\forall l\in\mathcal{L}^{sw} \quad (113)$$

$$\eta_l^7,\eta_l^8\ge0;\forall l\in\mathcal{L}\setminus\mathcal{L}^{sw}. \quad (114)$$

The first four summation terms in the objective function (73) represent the dual objective function of the lower-level problem (26)–(47). In addition, the last term in the objective function (73) expresses the product $\boldsymbol{\psi}^\top\boldsymbol{S}\hat{\boldsymbol{a}}^L$ as in (60). Please note that ψ is a fixed parameter in the subproblem, whose value comes from the first-stage solution. It is worth mentioning that vector $\boldsymbol{a}^L$ is an input parameter in $H(\boldsymbol{z}^{sw},\boldsymbol{a}^L)$. Nevertheless, by construction, vector $\boldsymbol{a}^L$ becomes a vector of decision variables in the subproblem. In this case, bilinear products involving $\boldsymbol{a}^L$ arise in the objective function (73). These products are replaced by different variables λ (each product has a different superscript over the symbol λ) and their corresponding linearizations are described through expressions (90)–(105).

Expressions (74)–(75) are the lower-level dual problem constraints associated with active and reactive power flow primal decision variables, respectively. Analogously, (76)–(78) are related to voltage variables, (78)–(81) correspond to active and reactive power flow variables, and (82)–(89) are associated with active and reactive deficit/surplus variables. Constraint (106) imposes a condition on vector $\boldsymbol{a}^L$ depending on the user defined parameter K, following the definition

of the support of $\boldsymbol{a}^L$ in (49). Finally, constraints (107)–(114) enforce non-negativity for the decision variables η (dual variables of the lower-level problem) that cannot assume negative values.

ACKNOWLEDGMENT

This work has been funded by the U.S. Department of Energy, Office of Electricity, under the contract DE-AC02-05CH11231.

REFERENCES

[1] L. Dale, M. Carnall, M. Wei, G. Fitts, and S. L. McDonald, "Assessing the impact of wildfires on the california electricity grid," California Energy Commission, Tech. Rep., August 2018.

[2] S. Li and T. Banerjee, "Spatial and Temporal Pattern of Wildfires in California from 2000 to 2019," *Scientific Reports*, vol. 11, 2021.

[3] B. D. Russell, C. L. Benner, and J. A. Wischkaemper, "Distribution feeder caused wildfires: Mechanisms and prevention," in *2012 65th Annual Conference for Protective Relay Engineers*, 2012, pp. 43–51.

[4] B. Chiu, R. Roy, and T. Tran, "Wildfire resiliency: California case for change," *IEEE Power Energy Mag.*, vol. 20, no. 1, pp. 28–37, 2022.

[5] M. Davoudi, B. Efaw, M. A. no Mora, J. L. Lauletta, and G. B. Huffman, "Reclosing of Distribution Systems for Wildfire Prevention," *IEEE Trans. Power Del.*, vol. 36, no. 4, pp. 2298–2307, August 2021.

[6] H. Nazaripouya, "Power Grid Resilience under Wildfire: A Review on Challenges and Solutions," in *2020 IEEE Power & Energy Society General Meeting*, August 2020, pp. 1–5.

[7] N. Romero, L. Nozick, I. Dobson, N. Xu, and D. Jones, "Transmission and Generation Expansion to Mitigate Seismic Risk," *IEEE Trans. Power Syst.*, vol. 28, no. 4, pp. 3692–3701, November 2013.

[8] T. Lagos, R. Moreno, A. N. Espinosa, M. Panteli, R. Sacaan, F. Ordonez, H. Rudnick, and P. Mancarella, "Identifying Optimal Portfolios of Resilient Network Investments Against Natural Hazards, With Applications to Earthquakes," *IEEE Trans. Power Syst.*, vol. 35, pp. 1411–1421, March 2020.

[9] M. Nazemi, M. Moeini-Aghtaie, M. Fotuhi-Firuzabad, and P. Dehghanian, "Energy Storage Planning for Enhanced Resilience of Power Distribution Networks Against Earthquakes," *IEEE Trans. Sustain. Energy*, vol. 11, no. 2, pp. 795–806, April 2020.

[10] Y. Lin and Z. Bie, "Tri-Level Optimal Hardening Plan for a Resilient Distribution System Considering Reconfiguration and DG Islanding," *Applied Energy*, vol. 210, pp. 1266–1279, January 2018.

[11] N. Rhodes, L. Ntaimo, and L. Roald, "Balancing Wildfire Risk and Power Outages Through Optimized Power Shut-Offs," *IEEE Trans. Power Syst.*, vol. 36, no. 4, pp. 3118–3128, July 2021.

[12] D. N. Trakas and N. D. Hatziargyriou, "Optimal Distribution System Operation for Enhancing Resilience Against Wildfires," *IEEE Trans. Power Syst.*, vol. 33, no. 2, pp. 2260–2271, 2018.

[13] D. L. Donaldson, M. S. Alvarez-Alvarado, and D. Jayaweera, "Power system resiliency during wildfires under increasing penetration of electric vehicles," in *2020 International Conference on Probabilistic Methods Applied to Power Systems (PMAPS)*, 2020, pp. 1–6.

[14] R. Moreno, D. N. Trakas, M. Jamieson, M. Panteli, P. Mancarella, G. Strbac, C. Marnay, and N. Hatziargyriou, "Microgrids against wildfires: Distributed energy resources enhance system resilience," *IEEE Power Energy Mag.*, vol. 20, no. 1, pp. 78–89, Jan.-Feb. 2022.

[15] M. Abdelmalak and M. Benidris, "Enhancing power system operational resilience against wildfires," *IEEE Trans. Ind. Appl.*, vol. 58, no. 2, pp. 1611–1621, Mar.-Apr. 2022.

[16] A. Arab, A. Khodaei, R. Eskandarpour, M. P. Thompson, and Y. Wei, "Three lines of defense for wildfire risk management in electric power grids: A review," *IEEE Access*, vol. 9, pp. 61 577–61 593, 2021.

[17] H. Nagarajan, E. Yamangil, R. Bent, P. Van Hentenryck, and S. Backhaus, "Optimal resilient transmission grid design," in *2016 Power Systems Computation Conference (PSCC)*, 2016, pp. 1–7.

[18] G. Byeon, P. Van Hentenryck, R. Bent, and H. Nagarajan, "Communication-constrained expansion planning for resilient distribution systems," *INFORMS Journal on Computing*, vol. 32, no. 4, pp. 968–985, 2020. [Online]. Available: https://doi.org/10.1287/ijoc.2019.0899

[19] R. Bayani and S. D. Manshadi, "Resilient expansion planning of electricity grid under prolonged wildfire risk," *IEEE Trans. Smart Grid.*, vol. 14, no. 5, pp. 3719–3731, Sep. 2023.

[20] E. A. Udren, C. Bolton, D. Dietmeyer, T. Rahman, and S. Flores-Castro, "Managing wildfire risks: Protection system technical developments combined with operational advances to improve public safety," *IEEE Power Energy Mag.*, vol. 20, no. 1, pp. 64–77, Jan 2022. [Online]. Available: https://ieeexplore.ieee.org/document/9675028/

[21] G. Huang, J. Wang, C. Chen, J. Qi, and C. Guo, "Integration of preventive and emergency responses for power grid resilience enhancement," *IEEE Trans. Power Syst.*, vol. 32, no. 6, pp. 4451–4463, Nov. 2017.

[22] Z. Bie, Y. Lin, G. Li, and F. Li, "Battling the extreme: A study on the power system resilience," *Proceedings of the IEEE*, vol. 105, no. 7, pp. 1253–1266, Jul. 2017.

[23] K. Wang, Y. Xue, Q. Guo, M. Shahidehpour, Q. Zhou, B. Wang, and H. Sun, "A coordinated reconfiguration strategy for multi-stage resilience enhancement in integrated power distribution and heating networks," *IEEE Trans. Smart Grid.*, vol. 14, no. 4, pp. 2709–2722, Jul. 2023.

[24] C. Chen, J. Wang, F. Qiu, and D. Zhao, "Resilient distribution system by microgrids formation after natural disasters," *IEEE Trans. Smart Grid.*, vol. 7, no. 2, pp. 958–966, Mar. 2016.

[25] S. Lei, C. Chen, Y. Song, and Y. Hou, "Radiality constraints for resilient reconfiguration of distribution systems: Formulation and application to microgrid formation," *IEEE Trans. Smart Grid.*, vol. 11, no. 5, pp. 3944–3956, Sep. 2020.

[26] A. Kavousi-Fard, M. Wang, and W. Su, "Stochastic resilient post-hurricane power system recovery based on mobile emergency resources and reconfigurable networked microgrids," *IEEE Access*, vol. 6, pp. 72 311–72 326, 2018.

[27] J. Muhs, M. Parvania, H. T. Nguyen, and J. A. Palmer, "Characterizing Probability of Wildfire Ignition Caused by Power Distribution Lines," *IEEE Trans. Power Del.*, pp. 1–8, 2020.

[28] V. Goel and I. E. Grossmann, "A Stochastic Programming Approach to Planning of Offshore Gas Field Developments under Uncertainty in Reserves," *Computers & Chemical Engineering*, vol. 28, no. 8, pp. 1409–1429, 2004.

[29] Y. Zhan, Q. P. Zheng, J. Wang, and P. Pinson, "Generation Expansion Planning With Large Amounts of Wind Power via Decision-Dependent Stochastic Programming," *IEEE Trans. Power Syst.*, vol. 32, no. 4, pp. 3015–3026, July 2017.

[30] W. Jahn, J. L. Urban, and G. Rein, "Powerlines and wildfires: Overview, perspectives, and climate change: Could there be more electricity blackouts in the future?" *IEEE Power Energy Mag.*, vol. 20, no. 1, pp. 16–27, Jan 2022. [Online]. Available: https://ieeexplore.ieee.org/document/9675048/

[31] F. Luo and S. Mehrotra, "Distributionally Robust Optimization with Decision Dependent Ambiguity Sets," *Optimization Letters*, vol. 14, no. 8, pp. 2565–2594, November 2020.

[32] S. Lee and Y. Ham, "Probabilistic framework for assessing the vulnerability of power distribution infrastructures under extreme wind conditions," *Sustainable Cities and Society*, vol. 65, p. 102587, Feb. 2021. [Online]. Available: https://www.sciencedirect.com/science/article/pii/S2210670720308052

[33] A. W. Dye, J. B. Kim, and K. L. Riley, "Spatial heterogeneity of winds during santa ana and non-santa ana wildfires in southern california with implications for fire risk modeling," *Heliyon*, vol. 6, no. 6, p. e04159, Jun. 2020. [Online]. Available: https://www.sciencedirect.com/science/article/pii/S2405844020310033

[34] J. A. Clavijo-Blanco and J. A. Rosendo-Macías, "Failure rates in distribution networks: Estimation methodology and application," *Electric Power Systems Research*, vol. 185, p. 106398, Aug. 2020. [Online]. Available: https://www.sciencedirect.com/science/article/pii/S0378779620302042

[35] J. Taylor and F. Hover, "Convex models of distribution system reconfiguration," *IEEE Trans. Power Syst.*, vol. 27, no. 3, pp. 1407–1413, Aug. 2012.

[36] M. Lavorato, J. F. Franco, M. J. Rider, and R. Romero, "Imposing radiality constraints in distribution system optimization problems," *IEEE Trans. Power Syst.*, vol. 27, no. 1, pp. 172–180, Feb. 2012.

[37] S. Mashayekh, M. Stadler, G. Cardoso, M. Heleno, S. Madathil, H. Nagarajan, R. Bent, M. Mueller-Stoffels, X. Lu, and J. Wang, "Security-Constrained Design of Isolated Multi-Energy Microgrids," *IEEE Trans. Power Syst.*, vol. 33, no. 3, pp. 2452–2462, 2018.

[38] A. Moreira, B. Fanzeres, and G. Strbac, "Energy and Reserve Scheduling under Ambiguity on Renewable Probability Distribution," *Electric Power Systems Research*, vol. 160, pp. 205–218, Jul. 2018.

[39] A. Moreira, G. Strbac, and B. Fanzeres, "An Ambiguity Averse Approach for Transmission Expansion Planning," in *2019 IEEE Milan PowerTech*, June 2019, pp. 1–6.

[40] A. Gupte, S. Ahmed, M. S. Cheon, and S. Dey, "Solving Mixed Integer Bilinear Problems using MILP Formulations," *SIAM Journal on Optimization*, vol. 23, no. 2, pp. 721–744, 2013.

[41] G. P. McCormick, "Computability of Global Solutions to Factorable Nonconvex Programs: Part I – Convex Underestimating Problems," *Mathematical Programming*, vol. 10, no. 1, pp. 147–175, Dec. 1976.

[42] A. Moreira, F. Piancó, B. Fanzeres, A. Street, R. Jiang, C. Zhao, and M. Heleno, "Distribution system operation amidst wildfire-

prone climate conditions under decision-dependent line availability uncertainty - dataset," 2023. [Online]. Available: https://dx.doi.org/10.21227/318q-5k50

[43] G. Muñoz-Delgado, J. Contreras, and J. Arroyo, "Multistage generation and network expansion planning in distribution systems considering uncertainty and reliability," *IEEE Trans. Power Syst.*, vol. 31, no. 5, pp. 3715–3728, 2016.

Alexandre Moreira (S'12–M'19) received the Electrical Engineering and Industrial Engineering degrees from the Pontifical Catholic University of Rio de Janeiro (PUC-Rio), Rio de Janeiro, Brazil, in 2011. He received his M.Sc. degree from the Electrical Engineering Department of PUC-Rio, in 2014, and his Ph.D. degree from the Department of Electrical and Electronic Engineering of the Imperial College London, London, UK, in 2019. He is currently a Research Scientist with the Lawrence Berkeley National Laboratory.

His research interests include decision making under uncertainty as well as power system economics, operation, and planning.

Felipe Piancó (S'18) received the B.S. degree in electrical engineering from the Rio de Janeiro State University (UERJ), Rio de Janeiro, Brazil, in 2021, and is pursuing the M.Sc. degree in industrial engineering at the Pontifical Catholic University of Rio de Janeiro (PUC-Rio), Rio de Janeiro, Brazil. He is currently an affiliate working with the Lawrence Berkeley National Laboratory (LBNL), California, USA. His research interests include power system planning, operation, resilience, and optimization.

Bruno Fanzeres (S'12–M'19) received the B.Sc. degree in industrial and electrical engineering and the M.Sc. and Ph.D. degrees in electrical engineering from the Pontifical Catholic University of Rio de Janeiro (PUC-Rio), Rio de Janeiro, Brazil, in 2011, 2014, and 2017, respectively.,He is currently an Assistant Professor with the Industrial Engineering Department, PUC-Rio, where he is also a Research Staff Member with the Laboratory of Applied Mathematical Programming and Statistics. His current research interests include data science techniques for signal processing and optical fiber monitoring as well as power systems operations and planning.

Alexandre Street (SM'17) received the M.Sc. and D.Sc. (Ph.D.) degrees in electrical engineering (emphasis in operations research) from the Pontifical Catholic University of Rio de Janeiro (PUC-Rio), Rio de Janeiro, Brazil.,From August 2006 to March 2007, he was a Visiting Researcher with the Universidad de Castilla-La Mancha, Ciudad Real, Spain. From 2003 to 2007, he participated in several projects related to strategic bidding in the Brazilian energy auctions and market regulation at the Power System Research Consulting, Rio de Janeiro. At the beginning of 2008, he joined the Electrical Engineering Department, PUC-Rio, where he is currently an Associate Professor and teaches energy economics, optimization, and statistics. He is one of the founders of the Laboratory of Applied Mathematical Programming and Statistics, where he is currently the Research Director of the Energy Group. His research interests include robust and stochastic models for power systems operation and planning, power system economics, renewable energy forecasting, and decision making under uncertainty. Prof. Street is a Senior Member of the IEEE Power and Energy Society and a CNPq Senior Scientist.

Ruiwei Jiang received the B.S. degree in industrial engineering from the Tsinghua University, Beijing, China, in 2009, and the Ph.D. degree in industrial and systems engineering from the University of Florida, Gainesville, FL, USA, in 2013. He is currently an Associate Professor with the Department of Industrial and Operations Engineering, University of Michigan, Ann Arbor, MI, USA. His research interests include power system planning and operations, renewable energy management, and water distribution operations and system analysis.

Chaoyue Zhao received the B.S. degree in information and computing sciences from Fudan University, Shanghai, China, in 2010, and the Ph.D. degree in industrial and systems engineering from the University of Florida, Gainesville, FL, USA, in 2014. She was an Assistant Professor in industrial engineering and management with Oklahoma State University, Stillwater, OK, USA. She is currently an Associate Professor in industrial and systems engineering with the University of Washington, Seattle, WA, USA. Her research interests include distributionally robust optimization and reinforcement learning with their applications in power system scheduling, planning, and resilience. In 2013, she was with Pacific Gas and Electric Company.

Miguel Heleno (SM'23) received the M.Sc. degree in electrical engineering and computer science from the University of Porto and the Ph.D. degree in sustainable energy systems from the same university within the MIT Portugal Program. He is currently a Research Scientist with the Lawrence Berkeley National Laboratory, leading research and innovation projects in the areas of power systems planning and economics.